

①

AD A124727



MEASUREMENT OF BARIUM EVAPORATION
FROM A DISPENSER CATHODE USING
LASER-INDUCED FLUORESCENCE

THESIS

AFIT/CEO/FH/82D-5

Eugene P. Kasper
Captain USAF

SEARCHED
SERIALIZED
FEB 23 1983
S E D

DTC FILE COPY

DEPARTMENT OF THE AIR FORCE
AIR UNIVERSITY (ATC)
AIR FORCE INSTITUTE OF TECHNOLOGY

Wright-Patterson Air Force Base, Ohio

83 02 022102

MEASUREMENT OF BARIUM EVAPORATION
FROM A DISPENSER CATHODE USING
LASER-INDUCED FLUORESCENCE

THESIS

AFIT/CEO/FH/82D-5

Eugene F. Kasper
Captain USAF

Approved for public release: distribution unlimited

AFIT/GEO/PH/82D-5

MEASUREMENT OF BARIUM EVAPORATION FROM A DISPENSER CATHODE
USING LASER-INDUCED FLUORESCENCE

THESIS

Presented to the Faculty of the School of Engineering
of the Air Force Institute of Technology
Air University
in Partial Fulfillment of the
Requirements for the Degree of
Master of Science

by
Eugene F. Kasper, B.S.E.E.
Captain USAF
Graduate Electro-Optics
December 1982

Accession For	
NTIS GRA&I	<input checked="checked" type="checkbox"/>
DTIC TAB	<input type="checkbox"/>
Unannounced	<input type="checkbox"/>
Justification	
By _____	
Date _____	
And _____	
Date _____	
A	

Approved for public release: distribution unlimited



Acknowledgements

There are several people who contributed in special ways to the completion of this project. I would like to thank:

Lt. Virginia Eason, U.S. Navy, whose advice on experimental technique enabled me to avoid many mistakes and blind alleys;

Capt. Arsenio T. Gumahad, U.S. Air Force, for his help in producing the computer-generated data plots;

Mr. Ron Gabriel of the AFIT Physics Department for his assistance in obtaining required equipment;

My thesis committee, Dr. Robert Hengehold, Dr. Ted Luke, and advisor Dr. Won Roh, for their advice, encouragement, and, sometimes, criticism which enabled me to keep the project on track and avoid getting trapped in inconsequentialities;

Finally, and most particularly, my wife Kyong Ae for her patience and many sacrifices during the period of this research which allowed me to keep my mind on my work.

Contents

	<u>Page</u>
Acknowledgements	ii
List of Figures and Tables	v
Abstract	vi
I. Introduction	1
General Comments	1
Statement of Purpose	2
Organization	2
II. Background.	4
Cathode Theory	4
Cathode Construction	7
Cathode Chemistry.	9
Cathode Operating Characteristics.	12
Laser-Induced Fluorescence in Barium	14
III. Equipment.	18
Laser Source	18
Vacuum System.	20
Test Cathodes.	21
Detection System	21
Wavelength Calibration Equipment	24
IV. Procedures.	26
Wavelength Calibration of the Laser Source	26
Adjustments of the Detection Electronics	27
Rayleigh Scatter Measurements to Determine $\Omega V_c \epsilon$	29
Measurement of the Barium Evaporation Rate	30
V. Results.	32
Counting Statistics.	32
Laser Scattering within the Test Cell	33
Blackbody Radiation from the Cathode	34
Photomultiplier Dark Current	35
System Signal to Noise Ratio	35
Propagation of Uncertainty through the Calculations.	36
Evaporation Rate versus Temperature.	37
Evaporation Rate versus Operating Time (Lifetime Test).	40
Comments on Accuracy	44

	<u>Page</u>
VI. Conclusions and Recommendations	46
Bibliography	48
Appendix A:Calculation of Laser Beam Diameter over Cathode	51
Appendix B: Tabulated Data	56

Lists of Figures and Tables

<u>Figure</u>		<u>Page</u>
1	Potential Energy Diagram of a Clean Metal	5
2	Dispenser Cathodes.	8
3	Simplified Energy Level Diagram of Barium I	15
4	Experimental System Diagram	19
5	Semicon Type S. Standard 300 Cathode.	22
6	Hollow-Cathode Tube Wavelength Monitor System . . .	25
7	Pulse-Height Analyzer Mode of Discriminator Operation.	28
8	Barium Evaporation Rate versus Cathode Temperature.	38
9	Barium Evaporation Rate versus Cathode Operating Time	41
9a	Barium Evaporation Rate during First Ten Hours of Operation	42
10	Laser Beam Path Schematic	54

<u>Table</u>		<u>Page</u>
1	Temperature Test Data	56
2	Operating Time Test Data.	56

10 to the 9th power

Abstract

The rate of evaporation of barium atoms from a thermionic dispenser cathode is measured as a function of cathode temperature and operating time using laser-induced fluorescence techniques. A continuous wave dye laser is tuned to the 5535⁶Å barium I transition, the laser beam is aimed over an operating cathode, and the resulting fluorescence is measured using photon counting techniques. The evaporation rate is then calculated from the measured fluorescent intensity.

The results indicate that for the Semicon type S cathode under test the evaporation rate increases until the cathode temperature reaches 1200⁶K, above which the rate decreases, possibly due to self absorption of the fluorescent photons inside the test cell. The lifetime data indicates that, after a high evaporation rate for the first 30 hours of operation, the evaporation rate decreases and becomes approximately constant at 7.11×10^5 atoms/sec for the 420 hour duration of the lifetime test. The cathode heater failed at 430 hours.

I Introduction

Solid-state electronic devices have displaced the electron tube for most applications. However, for high power microwave applications, the electron tube is still in wide use. In particular, the traveling-wave tube (TWT) is the primary transponder amplification element and the sole microwave power amplifier for communications satellites; as such, the TWT is among the satellite's basic life-limiting elements (Ref 1:387). In turn, the TWT's thermionic cathode is the tube's main life-limiting component.

A spaceborne cathode must fulfill several stringent requirements to ensure the TWT will have the required performance and lifetime characteristics. For example, the U.S. Air Force Space Division has established requirements for cathodes which include the ability to supply a current density of 1 to 2 amps/cm² for 60000 to 90000 hours (Ref 2:41).

A great deal of research was done on cathodes during the period of ascendancy of the vacuum tube. However, this research did not supply the knowledge required to reliably fabricate cathodes that could meet the rigid spaceborne requirements (Ref 2:5). Even now, as will be seen later in this report, some of the basic physics of cathode operations, particularly the role and structure of the barium layer on the cathode surface, is in dispute.

This experiment uses laser-induced fluorescence techniques to determine the evaporation rate of barium from a dispenser

cathode. The evaporating barium atoms absorb and reradiate photons from a laser beam whose wavelength is tuned to the barium $6s^2^1S_0 \rightarrow 6s6p^1P_1$ 5535⁰Å transition. The reradiated fluorescent photon counting rate is then related to the number density, evaporation flux, and evaporation rate of barium atoms. By varying the cathode temperature and by observing the barium evaporation rate over time, the relationships between the barium evaporation rate and cathode temperature and between the barium evaporation rate and operating time can be determined.

Statement of Purpose

The purpose of this experiment is to determine the evaporation rate of barium atoms from a dispenser cathode as a function of cathode temperature and operating time. These functional relationships should aid in the establishment of a model of the role of barium in cathode operation.

Organization

The remainder of this thesis consists of five chapters and two appendices. Chapter II presents the theory of dispenser cathode operation, construction, chemistry, and characteristics, along with a brief discussion on the technique of laser-induced fluorescence measurements. Chapter III discusses the equipment used in the experiment. Chapter IV describes the experimental procedures used. Chapter V presents the results of the experiment, along with an estimate of the experimental uncertainty. Chapter

VI summarizes the results of the experiment, draws available conclusions, and presents recommendations for additional research. Appendix A describes the calculations required to determine the diameter of the laser beam over the cathode and appendix B presents the experimental data in tabular form.

II Background

To understand the procedures used in this experiment and to interpret the results obtained, it is necessary to review the basic concepts of dispenser cathode operation and laser-induced fluorescence. This chapter will briefly survey the current knowledge of the theory, construction, chemistry, and operating characteristics of dispenser cathodes. Additionally, this chapter will present some considerations relating to the use of laser-induced fluorescence for the measurement of the barium evaporation rate from a dispenser cathode.

Cathode Theory

The purpose of a cathode in an electron tube is to supply an electron current which is controlled to produce a desired result. Since the current supplied by the cathode normally flows through the circuit's output load, a high output power requirement demands that the cathode supply a large current. Although not all cathodes are heated, this section will discuss electrically heated cathodes.

On the surface of a clean metal there exists a potential barrier which prevents the escape of low energy electrons. Figure 1 is a diagram of the potential barrier on a clean metallic surface. Electrons have an energy distribution described by the Fermi-Dirac distribution (Ref 3:151)

$$N(E)dE = \frac{g(E)dE}{1 + \exp((E-E_F)/kT)} \quad (1)$$

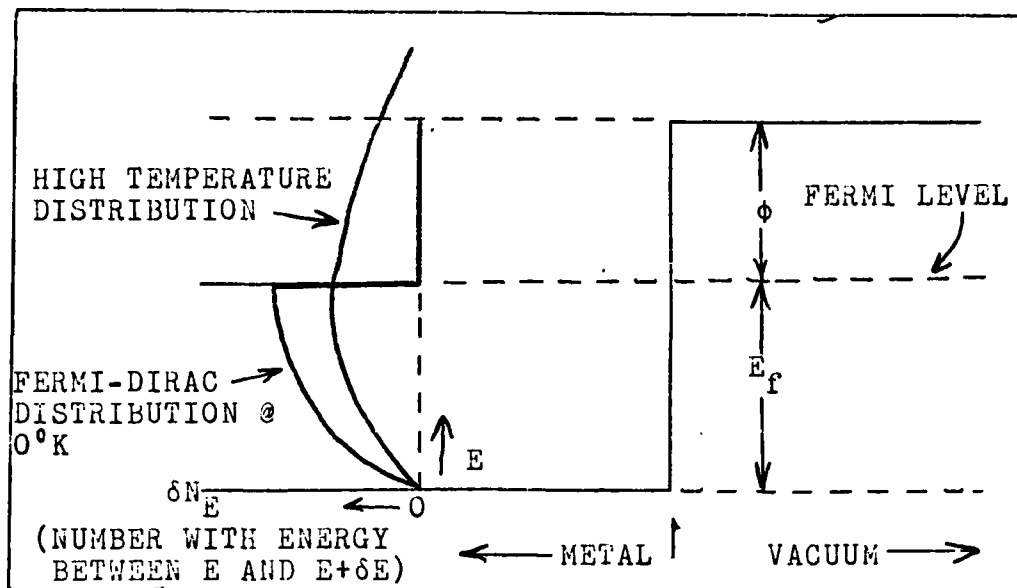


Figure 1. Potential Energy Diagram of a Clean Metal
(Ref 4:353)

where

$N(E)dE$ is the number of particles with energies between E and $E + \delta E$,

$g(E)$ is the density of states,

k is Boltzmann's constant (8.617×10^{-5} eV/°K), and

T is the temperature of the metal (°K).

From figure 1 and equation (1), it can be seen that at 0°K all electrons have energies less than or equal to the Fermi energy E_f . As the temperature increases, the distribution spreads out until, at a sufficiently high temperature, some electrons have energies great than $E_f + \phi$, where ϕ is the height of the potential barrier (i.e., the work function) at the surface; these electrons will be ejected from the surface. The current density resulting from these emitted electrons at a temperature T is given by the Richardson-Dushman equation (Ref 2:8-9)

$$J = AT^2 e^{-\phi/kT} \quad (2)$$

where

J is the electron current density (amps/cm²),

T is the temperature (°K),

φ is the work function (eV), and

A is the thermionic Richardson constant, 120 amps/cm²-°K².

Because of the inverse exponential relationship between φ and J, it is apparent that, to obtain large currents at reasonable temperatures, φ should be as low as possible. For example, tungsten has a work function of 4.56 eV (Ref 5:677). To obtain a current density of 1.0 amps/cm², the emitting surface would have to be raised to a temperature of approximately 2580°K. On the other hand, if the work function at the surface was reduced to 2.0 eV, the required temperature would only be 1220°K. The reduced temperature is advantageous in that less energy is required to heat the surface and that thermal stresses in the system are reduced. This example points out the desirability of lowering the work function if a large current density is required.

A way to reduce the work function of a metal is to deposit a layer of contaminant atoms which are electropositive with respect to the metal. This induces a polarization with the positive charge side outward; if the charge separation is a distance d with n contaminant atoms deposited per unit area, the work function is reduced by a factor $4\pi ned$ (Ref 4:354). This factor can reduce the work function by up to 3 eV which

would greatly increase electron emission at a given temperature. Although this effect is well-known and has been used to increase the electron emission from cathodes for as long as vacuum tubes have been used (Ref 6:1452), the physics involved remains somewhat hazy.

Cathode Construction

The major goal in cathode design and construction is to allow the formation of a layer of electropositive atoms, usually barium, on a metallic substrate which is usually tungsten. Two basic types of cathodes are in common use. The first is the oxide cathode which can supply continuous current densities of up to 0.3 amps/cm² at 750°C (Ref 2:15); it consists of a layer of barium strontium oxide on a very pure nickel substrate. The other general cathode type is the dispenser cathode, developed around 1949 (Ref 7:19), which can provide a few amps/cm² at temperatures of 1200-1400°K for several thousand hours (Ref 4:356). This section will concentrate on the construction and chemistry of the dispenser cathode.

There are two major types of dispenser cathodes (Ref 8:3-4). The L-cathode was developed in 1949 and consists of a porous tungsten disc which covers a cavity in a molybdenum shell; the cavity contains a mixture of barium and strontium carbonates (figure 2a). After assembly, the L-cathode is heated in vacuum; during heating, CO₂ is evolved from the carbonates, leaving mixed crystals of barium and strontium oxides. After CO₂ evolution is completed, the cathode is activated by further heating

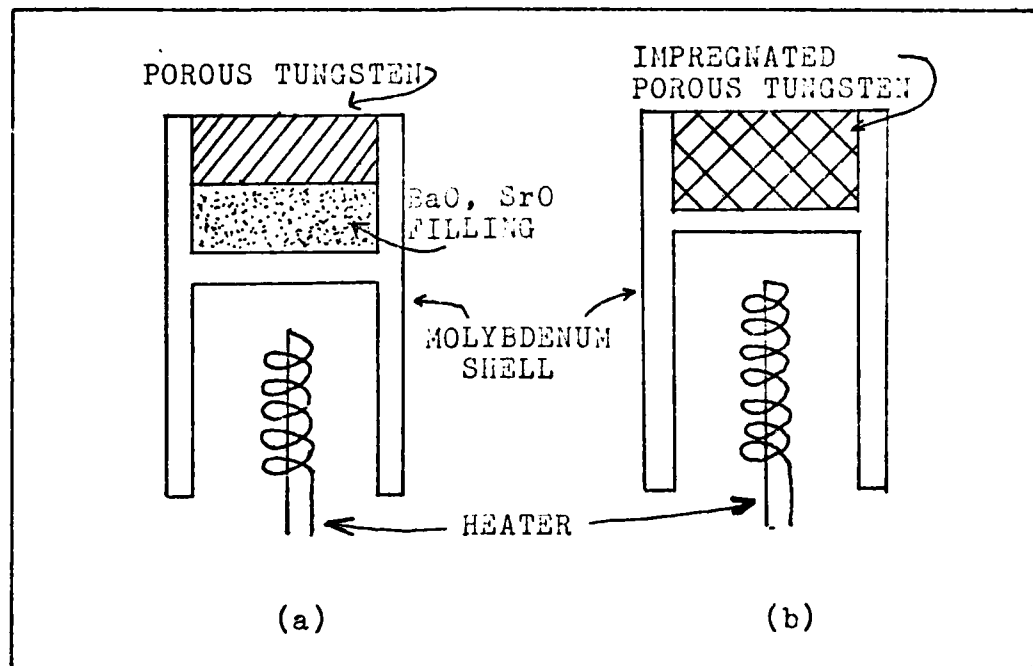


Figure 2. Dispenser Cathodes (Ref 4:356)
 (a) L-cathode
 (b) Flat Impregnated Cathode

at 1250°C to increase electron emission. The resulting L-cathode has a work function of 1.67 eV; the available current density at 1400°K is 4.7 amps/cm² (Ref 9:177-178). The L-cathode exhibits two major shortcomings: first, the pumping and activation times must be long to avoid oxidation of the tungsten; second, the chambered construction imposes limits on the size and shape of the L-cathode (Refs 4:357; 9:178). The impregnated cathode was developed to overcome these problems.

The impregnated cathode differs from the L-cathode in that the barium-generating compound is incorporated into the cavities of the porous tungsten during fabrication rather than being

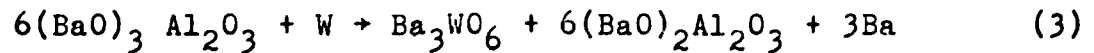
placed in a separate cavity (Ref 9:179). The modern form of the impregnated dispenser cathode consists of a porous tungsten plate; the pores are filled with barium calcium aluminate. The plate is brazed to a molybdenum shell (Ref 4:357) (figure 2b). The cathode is fabricated from high purity tungsten or tungsten-iridium powder with a controlled particle size of 2 - 14 μm . The powder is pressed into billets which are sintered in a hydrogen atmosphere. It can be seen that, by the choice of the mold used in the pressing of the billet, any desired size or shape of the cathode can be fabricated. The sintered billet is then machined into the desired shape. The impregnant compound is subsequently melted into the porous tungsten. Finally, the cathode is cleaned by grit blasting or polishing. The new cathode is activated by heating to 1225° C for a few hours. The activated cathode has a work function of 1.67 eV, which is the same as the L-cathode (Ref 7:21-22).

Other types of dispenser cathodes under study at this time include the M-cathode and the mixed-metal matrix cathode (Refs 7:23; 8:3-6). These cathode types show promise of higher current densities and longer lifetimes. However, since the impregnated cathode is widely used and was investigated in this experiment, the remainder of this chapter will discuss it.

Cathode Chemistry

Chemical reactions in the cathode convert the impregnant mixture, which is typically $4\text{BaO}:1\text{CaO}:1\text{Al}_2\text{O}_3$, $3\text{BaO}:1\text{CaO}:1\text{Al}_2\text{O}_3$, or $5\text{BaO}:3\text{CaO}:2\text{Al}_2\text{O}_3$ (Refs 7:22; 10), into free barium which is

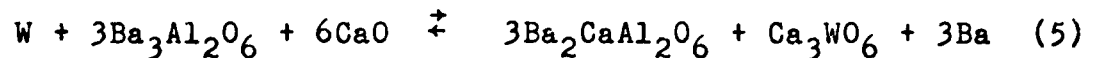
then deposited on the surface; this reduces the work function to the 2eV range. The reaction is of the form (Refs 4:357; 11:168)



The barium tungstate product in (3) can be further reduced (Ref 11:168)



The calcium also takes part in the reaction by (Refs 12:2898; 7:22)



In all of these reactions, free barium is the desired product. It diffuses through the pores of the tungsten billet and is deposited on the surface. However, the actual form of the surface layer is an area of much disagreement.

The structure of the emitting surface of the dispenser cathode is not well-established at this time. Although Zemyan (Ref 13:9) cites five models of the surface, the two models which have the widest acceptance are the model of a complete monolayer of barium on the surface which remains present for the cathode's entire life advanced by Rittner (Refs 14:165; 15:4346) and the model, favored by Forman, of a partial monolayer of barium which decreases in coverage over the life of the cathode (Ref 16:1547). The major cause of the disagreement is the differing results obtained in electron-emission versus

operating time experiments. Rittner (Ref 15:4345) shows a constant emission current density which implies a constant work function and, therefore, a constant coverage of the surface by the barium. On the other hand, Forman (Ref 16:1546), by using the cathode in a simulated TWT, shows a constant decrease of the emission current over time, thus indicating an increasing work function and a decreasing surface coverage. Surface analysis shows similarly divergent results; experiments at the Air Force Materials Laboratory using ion scattering spectrometry and secondary ion mass spectrometry indicate the surface is covered by a full monolayer (Ref 17:12), whereas experiments by Green at Varian, using high resolution Auger and X-ray photoelectron spectroscopy, indicated submonolayer coating (Ref 8:69).

Another aspect of cathode chemistry is the relationship among the barium, oxygen, and tungsten components. As the barium is transported through the porous tungsten structure, residual oxygen is picked up. Some of the oxygen is evaporated in the form of BaO (Ref 2:29-30); however, Haas, et al., using Auger and scanning low-energy electron probe techniques, have shown the emitting surface is more similar to a BaO structure on tungsten than to a pure barium on tungsten structure (Ref 18:3295). Green continued this research and developed a theoretical model of the bonding of barium to oxygen and oxygen to the tungsten surface d-orbitals. The ultimate test of this, or any of the other models proposed for the cathode structure, is the ability of the model to explain the known observations of cathode behavior.

Cathode Operating Characteristics

To be valid, a model of the cathode must be able to explain two major characteristics; the relationship between the barium evaporation rate over the lifetime of the cathode and the electron emission rate over the lifetime.

Since Rutledge, Milch, and Rittner published the results of their experiments (Ref 19:838), it has been well-accepted that the evaporation rate of barium from an impregnated cathode decreases with time as $t^{-\frac{1}{2}}$ (Refs 20:189; 2:31; 12:2897). In addition, Palluel and Shroff (Ref 12:2898) showed the barium depleted to a depth from the emitting surface also as $t^{-\frac{1}{2}}$. The decrease in the evaporation rate with time is attributed to the fact that, as the barium depletes from the emitting surface downward with time, the time required to reach the surface increases, thus decreasing the evaporation rate (Ref 12:2897).

The evaporation of barium can take place through two paths; barium can evaporate from the surface layer itself or through the pores of the tungsten (Ref 2:31). Rittner's data indicate the evaporation rate is low enough to permit a full monolayer of barium to cover the surface for the cathode's entire life (Ref 15:4344). Forman disagreed (Ref 16:1547) and stated that Rittner's low evaporation rate was due to the use of a close-spaced diode which permitted backscattering of barium from the anode to the cathode; using an open-gun structure similar to that used in TWT's, Forman's data indicated decreasing surface coverage by the barium. This is an interesting case in which the same basic observation, the $t^{-\frac{1}{2}}$ behavior in the barium

evaporation rate, can be interpreted in two different ways. However, the second basic characteristic to be explained by the model, the electron emission, shows very different behavior in different experiments.

Rittner and Forman also disagree on the basic behavior of the electron emission density over the lifetime of the cathode. Rittner, using the close-spaced diode, obtained a constant current density over time (Ref 15:4345) which is consistent with the full monolayer model. On the other hand, Forman shows a decrease in current density over time (Ref 16:1546) which is consistent with his decreasing coverage submonolayer model. Apparently, the different test conditions caused very different results; the lack of a standardized and accepted test procedure is a major obstacle to understanding cathode operation (Ref 2:42).

In this discussion of dispenser cathodes the basic theory and construction of the dispenser cathode were examined; it was also noted the chemistry, physical processes, and even the basic lifetime characteristics of the dispenser cathode are matters in dispute. It should also be noted that the research results have been primarily based either on inference (as in drawing conclusions regarding the barium layer based on data regarding electron emission) or on material analysis of non-operating cathodes. It would appear that a method of directly monitoring the relationship of the barium evaporation rate and the cathode's operating time would be useful in establishing a better model of the cathode; moreover, additional insights into the physical processes involved could be obtained. This experiment used

laser-induced fluorescence techniques to continuously and directly determine the barium evaporation rate from a cathode under operating conditions. The next subsection of this chapter will briefly discuss the use of laser-induced fluorescence in determining the barium evaporation rate.

Laser-Induced Fluorescence in Barium

Laser-induced fluorescence has been established as a method for the selective detection of small amounts of matter (Refs 21; 22). In particular, Zemyan (Ref 13) demonstrated the use of laser-induced fluorescence to measure the evaporation rate of barium from a dispenser cathode. Zemyan's method was used in this experiment to determine the evaporation rate-lifetime and evaporation rate-cathode temperature relationships. For a full discussion of the theory governing the laser-induced fluorescence of barium and a complete derivation of the equation relating fluorescence to the barium number density, see chapter III of Zemyan. The remainder of this subsection will briefly summarize his derivations.

In this experiment, a laser beam, tuned to the 5535\AA^0 $6s^2\ ^1S_0 \rightarrow 6s6p\ ^1P_1$ transition of barium I, is passed over a heated dispenser cathode. The barium atoms within the laser beam's volume over the cathode are excited into the 1P_1 state (figure 3). From the excited state, the barium atoms either decay into the ground state by emitting a fluorescent photon of 5535\AA^0 or into the metastable $6s5d\ ^1D_2$ state; the best current estimate of the branching ratio between the ground and the

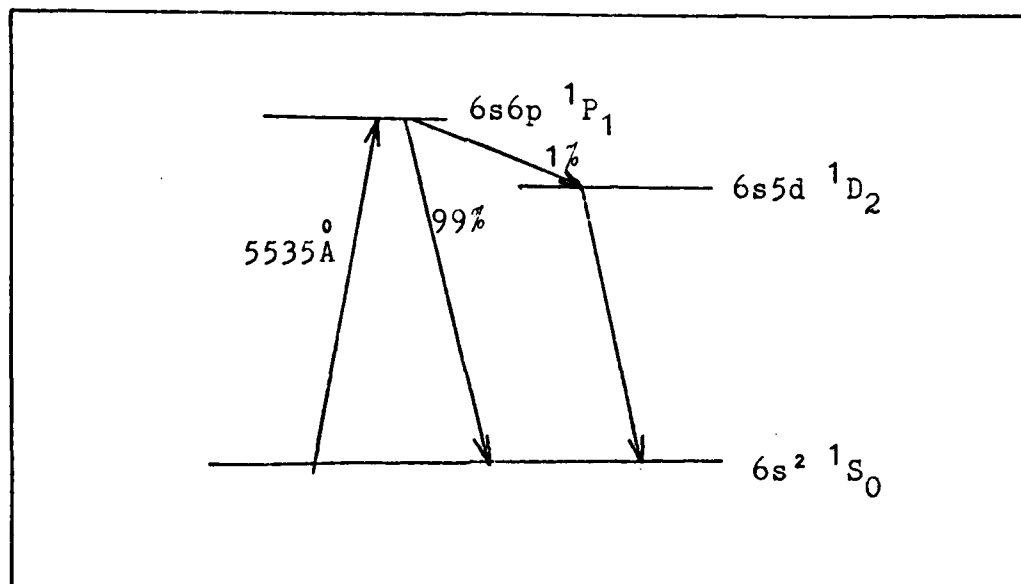


Figure 3. Simplified Energy Level Diagram of Barium I

metastable state is that 99% of the excited atoms will decay into the ground state (Ref 13:16). The lifetime of the $1D_2$ state is greater than 1 msec (Ref 22:269) and the barium atoms pass through the laser beam in approximately 2 μ sec, (Ref 13:17); therefore, atoms which decay into the metastable state do not participate in the fluorescence. Since the lifetime of the excited state is 8.2 nsec (Ref 23:A376) which is much less than the time the atoms are in the beam, each atom will, on average, emit 99 photons in the $1S_0 \rightarrow 1P_1 \rightarrow 1S_0$ cycle before it is pumped into the metastable state and lost to the system.

Using this line of reasoning, Zemyan developed the expression relating the number density of barium atoms within the laser beam volume to the detected fluorescent power (Ref 13:24)

$$N_t = (0.7) \frac{8\pi^2}{99} \frac{P_f}{h\nu} \frac{D}{v} \frac{1}{\Omega V_c \epsilon} \quad (6)$$

where

N_t is the number density of barium atoms (atoms/m³),

0.7 is a correction for the anisotropic fluorescence radiation (Ref 13:23, 59-61),

99 is the number of fluorescent photons emitted by each atom before decaying into the metastable state,

P_f is the detected fluorescent power,

$h\nu$ is the energy of the fluorescent 5535Å photons (3.519 x 10⁻¹⁹ J),

D is the laser beam diameter over the cathode (appendix A),

v is the rms speed of the barium atoms evaporating from the cathode,

Ω is the solid angle subtended by the detection optics,

V_c is the laser beam volume seen by the detection optics, and

ϵ is a correction factor which accounts for the overall efficiency of the photon counting system.

Since $P_f/h\nu$ is the counting rate of the fluorescent photons detected by the photon counting system, equation (6) can be rewritten as

$$N_t = (0.7) \frac{8\pi^2}{99} \frac{R_f D}{v} \frac{1}{\Omega V_c \epsilon} \quad (7)$$

where R_f is the measured fluorescent count rate. Since $\Omega V_c \epsilon$ can be determined by a Rayleigh scattering measurement (Refs 13:20, 62-63; 21:8-9,20), only R_f need be measured to determine N_t . Once N_t is determined, the evaporation flux F_e can be calculated by (Ref 13:49)

$$F_e = N_t v \text{ (atoms/m}^2\text{-sec)} \quad (8)$$

Finally, the evaporation rate R_e is determined from F_e

$$R_e = F_e A_e \text{ (atoms/sec)} \quad (9)$$

where A_e is the area of the emitting cathode surface.

Equations (7), (8), and (9) are the relationships used to convert the experimentally determined quantity R_f into the desired quantity R_e . The next chapter of this thesis will discuss the equipment used to measure R_f .

III Equipment

This chapter describes the experimental apparatus used to induce and detect fluorescence from the barium atoms emitted from the test cathode. The major elements in the setup were the laser source, the vacuum system, the test cathodes, the detection system, and the wavelength calibration equipment; each of these elements will be individually discussed. An overall diagram of the system is shown in figure 4.

Laser Source

The source of laser light used to induce fluorescence was a Spectra-Physics model 375 continuous wave dye laser which was pumped by a Spectra-Physics model 164 argon ion laser. The dye laser used Rhodamine 560 dye and was equipped with a birefringent filter for tuning and a 0.1mm thick quartz etalon for line narrowing. Together, the filter and etalon provided a laser linewidth of 11.3 GHz as measured by an external Fabry-Perot analyzer; this linewidth corresponds to a wavelength spread of 0.115\AA ⁰. Maximum dye laser output power was 300 mW continuous, although the power used in this experiment was held to 250 mW maximum due to a 30 amp limit on the laboratory AC mains which limited the maximum output power from the pump laser, thus limiting dye laser output.

The laser beam was chopped by a Princeton Applied Research (PAR) 125A mechanical chopper which was set for a chopping frequency of 169 Hz. The chopper also provided a synchronizing

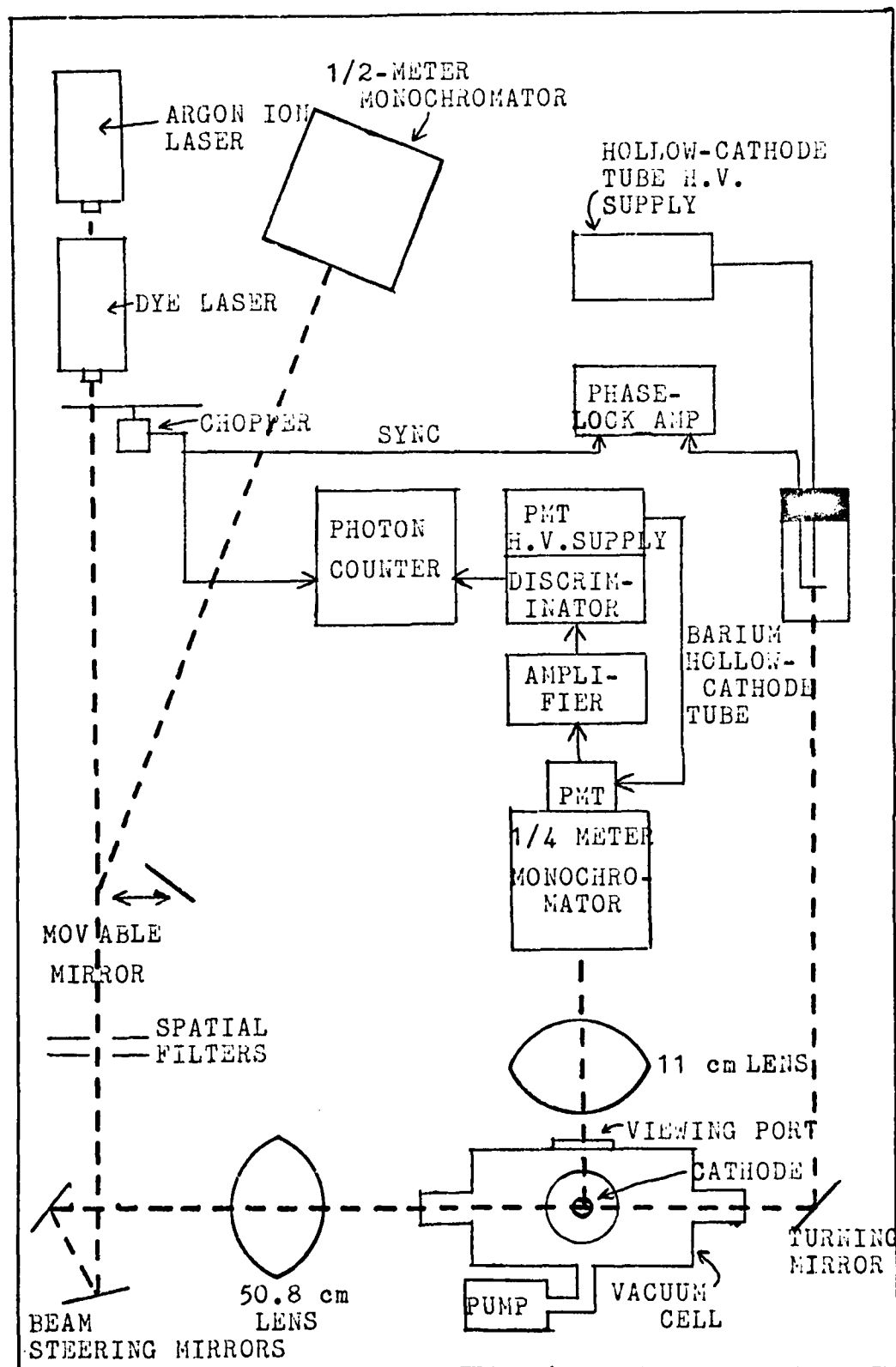


Figure 4. Experimental System Diagram

signal to the photon counter and phase-lock amplifier used in the detection and calibration equipment. The chopped laser beam permitted the use of an automatic background subtraction mode of photon counter operation, and the synchronizing signal locked the photon counter and phase-lock amplifier onto the laser beam's on-off cycle. The automatic background subtraction mode will be discussed in detail in the section dealing with the photon counter.

Vacuum System

The vacuum system consisted of a Varian vacuum chamber, two Varian Vac-Sorb[®] absorption pumps and a mechanical vacuum pump with an oil trap for rough pumping of the vacuum chamber to the one micron range, a Varian 80 liter/second Vac-Ion[®] pump and controller for final pumping to the 10^{-8} torr range, and a liquid nitrogen cooled cold finger in the vacuum cell to trap as much material evaporating from the cathode as possible. Together, the Vac-Ion pump and the cold finger were able to maintain a pressure in the cell in the 10^{-8} torr range with the cathode heated. The vacuum chamber was equipped with a leak valve in the roughing manifold which permitted filling the cell with nitrogen gas for the Rayleigh scattering measurements to determine ΩV_{cs} . The cathode and fluorescing volume were observed through a glass viewing port. The cathode under test was mounted in the vacuum cell by use of a flange and vacuum bellows which permitted minor adjustments of the cathode position with respect to the laser beam and provided vacuum feed-throughs for the electrical connections to the cathode.

Test Cathodes

Two test cathodes were used in this experiment. The first, used for evaporation rate versus cathode temperature tests, was the same one used by Zemyan (Ref 13:33-34) in his research; the second, used for the evaporation rate versus operating time tests, was a new sample. Both were Semicon Associates type S dispenser cathodes (Figure 5). The cathodes consisted of an impregnated porous tungsten plug attached to a molybdenum shell. The tungsten density was $82 \pm 0.4\%$; the impregnant composition (mole ratio) was $4\text{BaO} : 1\text{CaO} : 1\text{Al}_2\text{O}_3$ (Ref 10). Specifically, the sample used for the lifetime test was serial number 2, job number 4331, impregnant lot number 5428, with a weight gain due to the impregnant mix of 0.0302 grams. Note the molecular weight of the impregnant mix is 707.364 grams/mole; therefore, the cathode absorbed 4.269×10^{-5} mole of the impregnant mix. From this, it can be shown that 1.708×10^{-4} mole, or 0.023 grams, of barium was absorbed during impregnation.

The samples were prepared by spot welding (electric arc) the heater and support wires to the wires leading to the vacuum feedthroughs on the flange-bellows assembly mentioned above. In addition, a type K (chromel/alumel) thermocouple was also spot-welded to the cathode body and the thermocouple leads also brought out through the vacuum feed-throughs.

Detection System

The detection system consisted of an 11 cm focal length lens, a Jarrell-Ash 1/4 - meter monochromator, an RCA type 8850

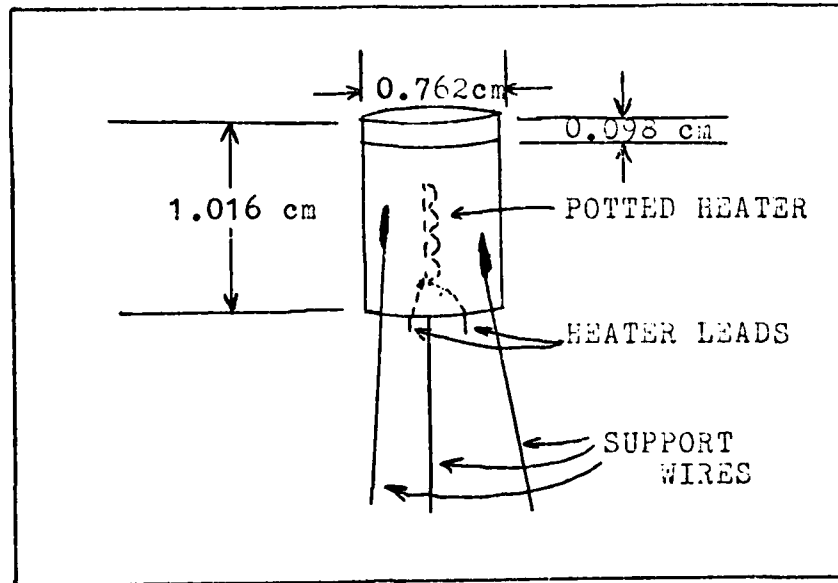


Figure 5. Semicon Type S, Standard 300 Cathode

photomultiplier tube (PMT), a Princeton Applied Research (PAR) model 1121A amplifier/discriminator, a PAR HVS-1 PMT high voltage supply, and a PAR 1112 photon counter/processor.

The lens was chosen and positioned to image the cathode and fluorescing volume onto the entrance slit of the monochromator. The 1/4 - meter monochromator itself served to filter out the black-body radiation from the hot cathode outside the wavelength region of interest; this reduced the background affecting the PMT. The area of the vertically oriented 500 micron wide entrance slit on which the cathode was imaged was blocked off to further reduce extraneous background. The PMT, in turn, was mounted on the monochromator exit slit with a lightproof seal. The optical path from the observation port to the monochromator was covered by a black box which minimized the effects of room lights and scattered laser light on the PMT.

The signal from the PMT was fed into the PAR 1121A amplifier/

discriminator. This device performed four functions: first, the HVS-1 circuit board in the 1121A provided the high voltage bias to the PMT and permitted monitoring of the high voltage level; second, it amplified and conditioned the output of the PMT to a form acceptable to the photon counter; third, by use of the threshold level settings, it discriminated between PMT output due to the desired fluorescent signal and that due to noise; and, fourth, it provided a divide-by-ten prescale function to avoid overload of the discriminator due to rapidly arriving PMT output pulses and the resulting loss of some output pulses.

The output of the discriminator was then fed into the PAR 1112 photon counter/processor. In addition, the synchronizing signal from the mechanical chopper was applied to the 1112's chop trigger input. The purpose of the 1112 is to count and display the output pulses from the discriminator and, therefore, from the PMT. In this experiment, the 1112 was operated in the "chop" or automatic background subtraction mode; this permitted the automatic subtraction of the background signal from the total light (i.e., signal plus background) signal to give the net fluorescent output. To do this, when the synchronizing signal from the chopper was high, the laser beam was blocked ("off") and the pulses from the discriminator were counted in a background register since the pulses were due only to the background; when the chopper output signal was low, the laser beam was unblocked ("on") and the discriminator output pulses were counted in a signal-plus-background register. The contents of the two

registers could be displayed individually; the 1112 could also display the sum of the register contents or the difference between the two which was the net signal.

The difference displayed by the 1112 consisted of two parts: the actual fluorescent signal and laser light scattered inside the test cell. Since the scattered light also turned on and off in synchronization with the fluorescent signal (since both were caused by the laser beam), the 1112 could not discriminate between the desired fluorescent signal and scattered laser light. To overcome this, a measurement of the intensity of the scattered light was taken with the cathode heater off. By assuming the intensity of the scattered light was not a function of the cathode temperature, the scattered photon count rate could be directly subtracted from the difference displayed by the 1112 to give the true net fluorescent signal.

Wavelength Calibration Equipment

The equipment used to monitor the wavelength of the laser light consisted of a 1/2 - meter Jarrell-Ash monochromator, a Jarrell-Ash barium-neon hollow-cathode tube, an Ithaco Research 353 phase-lock amplifier, a Hewlett-Packard 712B high voltage supply for the hollow-cathode tube, and an R-C coupling network for the tube.

The procedure for tuning the laser had two steps. The coarse tuning was accomplished by directing the laser beam into the 1/2 - meter monochromator input and adjusting the dye laser's birefringent filter and etalon for the brightest monochromator

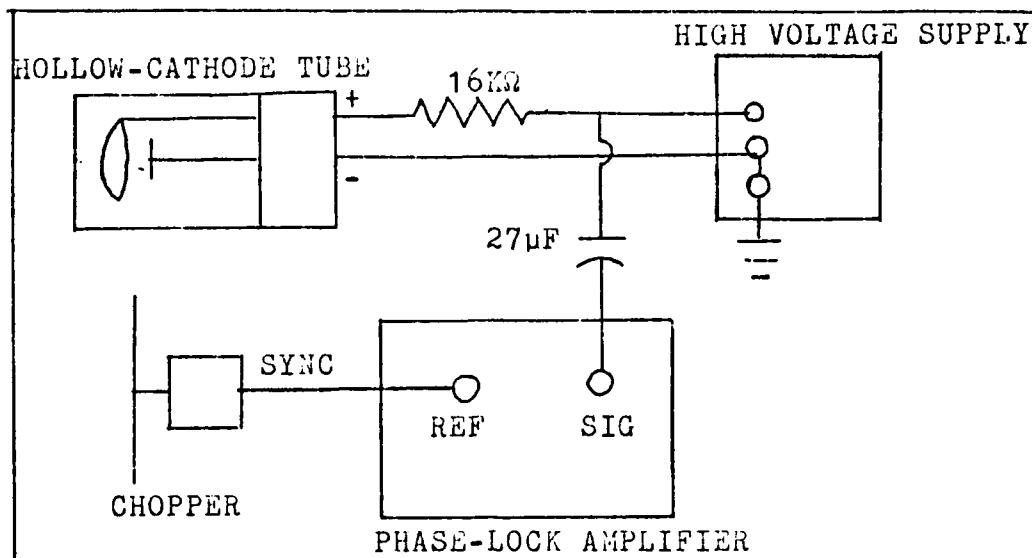


Figure 6. Hollow-Cathode Tube Wavelength Monitor System

output beam with the monochromator tuned to 5535\AA . For fine tuning, the laser beam was directed into the hollow-cathode tube which was biased at 370 volts (Figure 6). Through the optogalvanic effect, discussed in detail in Zemyan (Ref 13: 27-32), the tube generated an output voltage dependent on the incident power and wavelength. This output voltage varied in synchronization with the chopper signal. The hollow-cathode tube output and the chopper sync signal were both applied to the phase-lock amplifier which detected the optogalvanic signal in phase with the chopper sync signal, amplified the optogalvanic signal, and displayed the amplified voltage on a panel meter. This system permitted continuous monitoring of the laser wavelength during measurements, although the dye laser showed little tendency to drift off frequency once tuned.

IV Procedures

This experiment had four major elements: the wavelength calibration of the laser source, the adjustments of the detection electronics, the Rayleigh scattering measurements to determine the system parameter ΩV_c , and the actual measurements of the barium evaporation rate. This chapter will discuss each element individually.

Wavelength Calibration of the Laser Source

The purpose of the calibration of the dye laser was to insure the laser light was at the $5535\overset{0}{\text{\AA}}$ wavelength necessary to excite the barium $6s^2\ ^1S_0 \rightarrow 6s6p\ ^1P_1$ transition. A two-step calibration procedure, using a monochromator for rough tuning and a hollow-cathode barium tube for fine tuning, was found to be effective for this experiment.

The rough tuning was accomplished using a 1/2 - meter Jarrell-Ash monochromator. The monochromator was first calibrated around the barium line wavelength using mercury and krypton calibration lamps. From the known spectral lines of the calibration sources, a calibration chart for the monochromator was constructed. The accuracy of the chart was checked by using a neon lamp as a test source; the wavelengths obtained from the monochromator through the calibration chart agreed with published values to within $0.5\overset{0}{\text{\AA}}$. The monochromator setting for the barium $5535\overset{0}{\text{\AA}}$ line was then interpolated from the calibration chart and the monochromator was set to that wavelength. The dye

laser beam was then directed into the monochromator; the output wavelength was adjusted by use of the birefringent filter and etalon until the monochromator output was maximized, thus indicating the proper wavelength.

The fine tuning was accomplished by directing the dye laser beam into the barium hollow-cathode tube. With the mechanical chopper supplying a reference signal to the phase-lock amplifier and the output voltage from the barium tube connected to the amplifier input, the birefringent filter and etalon were adjusted to obtain the maximum output voltage from the barium tube as displayed on the phase-lock amplifier. It should be noted that the hollow-cathode tube was filled with neon; as a result, the amplifier also showed an output voltage from the tube with the laser tuned to the neon 5533.7\AA^0 and 5538.7\AA^0 lines. These lines bracketed the barium transition of interest and provided another check on the accuracy of the monochromator calibration chart.

Adjustments of the Detection Electronics

The adjustments of the photomultiplier tube (PMT) high voltage supply, the amplifier/discriminator threshold levels, and the photon counter timing intervals were made in order to maximize the output due to the desired fluorescent signal and minimize the effects of noise.

The high voltage supply of the PMT was adjusted in accordance with the instruction manual of the Princeton Applied Research (PAR) 1121A amplifier/discriminator (Ref 25: IV-5,

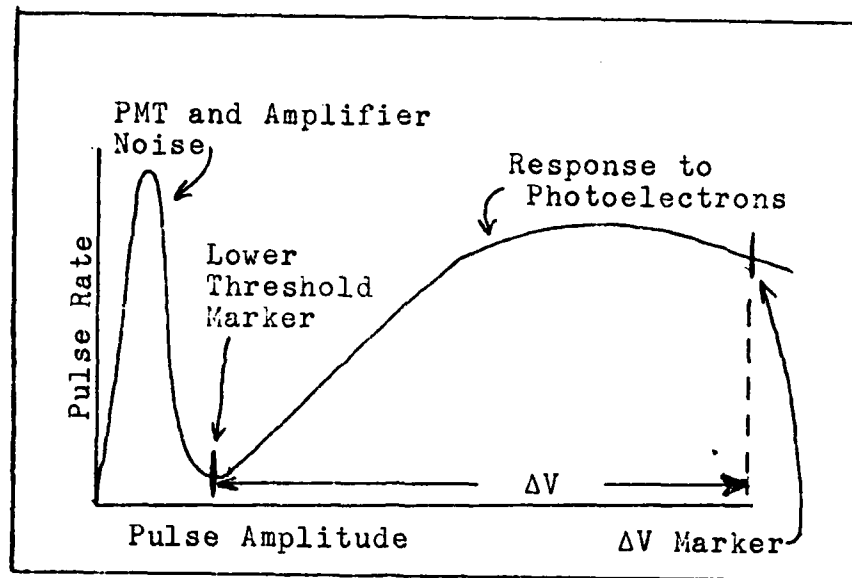


Figure 7. Pulse-Height Analyzer Mode of Discriminator Operation

figure IV-2). With the 1121A set for the pulse-height analyzer (PHA) mode of operation and a 7.5 watt light bulb used as the light source, the high voltage was adjusted until an oscilloscope trace similar to figure 7 was obtained. The high voltage required to obtain the optimum PHA response was 1659 volts; this value of PMT supply voltage was used for the rest of the experiment.

The threshold levels on the amplifier/discriminator were then set. With the 1121A still in the PHA mode, the lower threshold level marker was set in the valley between the peaks due to noise and photoelectron response; the ΔV (the difference between the lower and upper thresholds) marker was set beyond the peak due to the photoelectrons. The effect of these adjustments was to set the discriminator to reject input pulses due to noise and extremely high level signals, thus passing to the

photon counter only those PMT pulses due to the desired fluorescent signal. The lower threshold level was set to 0.7mV, with ΔV set to 2.5 mV.

The adjustments on the PAR 1112 photon counter synchronized the counter with the chopper reference signal. Since the chopping frequency was 169 Hz, the chopping period was 5.92 milliseconds. Because the laser beam was passed for 50% of the chopping period, the beam was passed for 2.96 msec. In accordance with the instructions for the 1112 (Ref 26: IV-6), the sample interval was set to the nearest lower 0.1 msec; therefore, the sample interval was set to 2.9 msec. The "preset N" control on the 1112 set the number of intervals sampled. For convenient interpretation of results, it was decided to use sample times of one, ten, or one hundred seconds. Since the chopper wheel was set for 169 Hz, the desired sample times resulted in 169, 1690, or 16900 samples to be counted for the corresponding sample times; these numbers of samples were entered into the "preset N".

Rayleigh Scatter Measurements to Determine ΩV_{ce}

The system parameter ΩV_{ce} was determined by the method of Benham (Ref 21: 8-9,20) and Zemyan (Ref 13:20,62-63). The test cell was backfilled to 760 torr with nitrogen gas. A laser beam was then passed through the cell and the Rayleigh scattered light was measured with the detection system. With an input laser power of 250 mW, (16480 ± 256) counts/second were obtained. Using the equation from Zemyan (Ref 13:62), the parameter was

calculated by

$$\Omega V_c \epsilon = \frac{P_R}{N_n} \frac{A_\lambda}{P_\lambda} \frac{1}{d\sigma/d\Omega} \quad (10)$$

where

P_R is the received (scattered) power (W),

N_n is the nitrogen gas number density (m^{-3}),

A_λ is the laser beam cross-sectional area (m^2),

P_λ is the input laser power (W), and

$d\sigma/d\Omega$ is the differential scattering cross-section for N_2 ,

given by George, et al. (Ref 27:4379) as

$$1.04 \times 10^{-32} \text{ m}^2/\text{steradian}.$$

Using the measured count rate, $\Omega V_c \epsilon$ was calculated to be

$$(4.189 \pm 0.082) \times 10^{-14} \text{ m}^3\text{-steradian}.$$

Measurement of the Barium Evaporation Rate

The barium evaporation rate was measured by counting the photons emitted from the fluorescent volume above the cathode for 100 seconds, converting the count into a count rate R_f in fluorescent photons/second, and, by use of the relationship discussed in Section II

$$N_t = 0.7 \frac{8\pi^2 R_f}{99} \frac{D}{v} \frac{1}{\Omega V_c \epsilon} \quad (7)$$

converting the fluorescent count rate into a barium number density N_t . In turn, the evaporation flux F_e and the evaporation rate R_e were calculated from N_t by the relationships

$$F_e = N_t v \quad (\text{atoms/m}^2\text{-sec}) \quad (8)$$

and

$$R_e = F_e A_e \quad (\text{atoms/sec}) \quad (9)$$

where

v is the thermal velocity of the barium atoms and

A_e is the area of the emitting surface.

To take a measurement of the barium evaporation rate the desired temperature or time condition on the cathode was established, the dye laser output was adjusted to 5535⁰A using the procedures outlined above, the input power was adjusted to 200 mW, and the photon counter was started. The photon counter sampled the fluorescent-signal-plus-background and background-only for 100 seconds and displayed the difference (i.e., the number of fluorescent photons counted). After the 100-second sample, the input power was rechecked. Ten 100-second samples were taken for each time or temperature condition; the mean and standard deviation of the number of photons counted were calculated for each ten sample set. The mean number of fluorescent photons was then converted into an evaporation rate using the relationships above.

Measurements of the barium evaporation rate were taken for cathode temperatures from 900°K to 1300°K and for 430 hours of operation at 1200°K. The results of these measurements are discussed in the next section.

V Results

The results of interest of this experiment are the barium evaporation rate-cathode temperature and barium evaporation rate-operating time relationships. The measured quantity was the photon count due to the laser-induced fluorescence of the evaporating barium atoms. From this the barium number density, the evaporation flux, and the evaporation rate were calculated.

The photon count consisted not only of the desired fluorescent photons but also of laser photons scattered from the environment within the test cell, blackbody radiation from the cathode, and pulses due to PMT dark current. In addition, the standard deviation in a set of measurements reflect an inherent uncertainty in the measuring process. This chapter will briefly discuss these sources of error, estimate the magnitude of each, and present and interpret the calculated values of the barium evaporation rate.

Counting Statistics

Modern photomultiplier tubes have dynode gain distributions and photoelectron emission characteristics which reflect Poisson statistics (Ref 25:II-11). A Poisson distribution gives the probability $P(x)$ of an event occurring exactly X times in a specific time interval t (Ref 25:II-3). For a Poisson distribution about a mean value \bar{x} , the standard deviation of the measurement is $(\bar{x})^{\frac{1}{2}}$. To calculate the standard deviation of a count rate, one takes the standard deviation of the number of counts

and divides by the counting time. That is

$$\sigma_R = \sigma_X / t \quad (11)$$

where σ_R is the standard deviation in the count rate, σ_X is the standard deviation in the number of counts, and t is the time over which the measurement was taken (Ref 13:42). In this experiment the photons were counted over 100 seconds; because the discriminator provided a divide-by-ten prescaling in the number of counts, the net effect was that of a 10 second count.

Each measurement in this experiment consisted of ten 100-second count cycles. The difference reading given by the photon counter was noted for each count cycle, along with the signal-plus-background and background readings. A mean value for the ten count cycle set was calculated along with the standard deviation. To obtain a count rate per second, the mean was divided by the counting period and, as indicated in equation (11), the standard deviation of the count rate was calculated by dividing the standard deviation of the difference count by ten. This value of the photon count rate per second and its corresponding standard deviation was the raw data for each temperature or time sample.

Laser Scattering Within the Test Cell

Because of such mechanisms as reflections from the Brewster's windows in the test cell, scattering from surfaces inside the test cell, and light scattered from the optical chain entering the test cell, a certain number of the counted photons do not

come from the fluorescing volume. Since these scattered photons have the same wavelength as the fluorescent photons, no direct discrimination is possible. Scattering was reduced by accurate alignment of the laser beam through the test cell and by enclosing the detection optics in a light shield. The residual scattering was accounted for by counting the scattered photons with the cathode heater off; this value was subtracted from the raw photon count discussed above to give a net photon count rate. This scatter was measured to be $(1.765 \pm 0.032) \times 10^3/\text{second}$, and was in the order of five to ten percent of the fluorescent count rate.

Blackbody Radiation from the Cathode

As a heated source, the cathode emits blackbody radiation, some of which lies within the wavelength passband of the 1/4-meter monochromator. Even with the filtering provided by the monochromator, the number of photons emitted from the cathode may be enough to overload the detection electronics. To minimize this effect, the part of the monochromator input slit on which the cathode was imaged was covered by black tape. However, since the interior of the test cell was reflective, a number of blackbody photons still appeared as background.

The photon counter's "chop" mode provided a method for evaluating this background radiation. As discussed earlier in this report, the photon counter evaluates separately the number of signal-plus-background photons and the background

only photons and subtracts the two. The difference is the fluorescent signal. This value was recorded along with the signal-plus-background and background-only readings.

Photomultiplier Dark Current

Because of the high gain of the PMT, random thermal generation of electrons from the photocathode can cause a significant number of output pulses from the PMT. The discriminator cannot distinguish between the pulses due to thermal emission from those caused by the desired fluorescent photons; however, since the dark current pulses existed for both the signal-plus-background and background-only conditions, the "chop" mode of the photon counter was able to account for the dark current. It should be noted that, with the PMT bias and discriminator threshold levels set as described in section IV, a dark current count rate of $(1005 \pm 49)/\text{second}$ was obtained; since this rate was in the order of two to five percent of the obtained photon count rate, no cooling of the PMT was considered necessary.

System Signal to Noise Ratio

Using a photon counting system with automatic background subtraction as was utilized in this experiment, the output noise in the system is given by (Ref 25:II-11)

$$\text{NOISE} = \left[\left(\frac{\text{SIGNAL}}{\text{COUNT}} + \frac{\text{BACKGROUND}}{\text{COUNT}} \right) + \frac{\text{BACKGROUND}}{\text{COUNT}} \right]^{\frac{1}{2}} \quad (12)$$

so that the signal to noise ratio is

$$\frac{S}{N} = \frac{(\text{SIGNAL COUNT} + \text{BACKGROUND COUNT}) - \text{BACKGROUND COUNT}}{((\text{SIGNAL COUNT} + \text{BACKGROUND COUNT}) + \text{BACKGROUND COUNT})^{\frac{1}{2}}} \quad (13)$$

Since the signal-plus-background, background, and signal-only values were available from the photon counter, each was recorded. By evaluating the above equations, the signal to noise ratio in the system was found to be approximately 15.

Propagation of Uncertainty through the Calculations

The effect of random noise and variations of the fluorescent counts with a measurement set is to introduce an uncertainty as to the actual value of the fluorescent count rate. Since the desired information, the evaporation rate, must be calculated from the measured fluorescent count rate, the effect of the uncertainty in the quantity on the final result must be determined.

If the uncertainties in two measurements x and y are expressed by standard deviations σ_x and σ_y , the uncertainty in a functional combination (sum, difference, etc.) is not simply the same function applied to σ_x and σ_y individually. For example, if

$$z = x + y \quad (14)$$

then

$$\sigma_z \neq \sigma_x + \sigma_y \quad (14)$$

Rather

$$\sigma_z = (\sigma_x^2 + \sigma_y^2)^{\frac{1}{2}} \quad (15)$$

Similarly, for other functional combinations (Ref 28:A2/11)

$$z=x-y \quad \sigma_z=(\sigma_x^2 + \sigma_y^2)^{\frac{1}{2}} \quad (16)$$

$$z=xy \quad \sigma_z=z((\sigma_x/x)^2 + (\sigma_y/y)^2)^{\frac{1}{2}} \quad (17)$$

$$z=x/y \quad \sigma_z=z((\sigma_x/x)^2 + (\sigma_y/y)^2)^{\frac{1}{2}} \quad (18)$$

The equation relating the fluorescent count rate to the number density of barium is repeated:

$$N_t = (0.7) \frac{8\pi^2 R_f}{99} \frac{D}{v} \frac{1}{\Omega V_c \epsilon} \quad (7)$$

Since the equation involves products and quotients only, the uncertainties present in R_f , v (through the variation in cathode temperature), and $\Omega V_c \epsilon$ propagate as

$$\sigma_{N_t} = N_t((\sigma_A/\Omega V_c \epsilon)^2 + (\sigma_{R_f}/R_f)^2 + (\sigma_{T_c}/T_c)^2)^{\frac{1}{2}} \quad (19)$$

where

σ_{N_t} is the standard deviation in the number density

σ_A is the standard deviation of the factor $\Omega V_c \epsilon$

σ_{R_f} is the standard deviation in the fluorescent count rate and

σ_{T_c} is the uncertainty in the cathode temperature.

Using the measured or assumed values for the standard deviations σ_A , σ_{R_f} , and σ_{T_c} , σ_{N_t} was found to be 5 to 11% of the calculated number density and averaged about 7%.

Evaporation Rate versus Temperature

The relationship between the barium evaporation rate and the cathode temperature is shown in figure 8. The values ob-

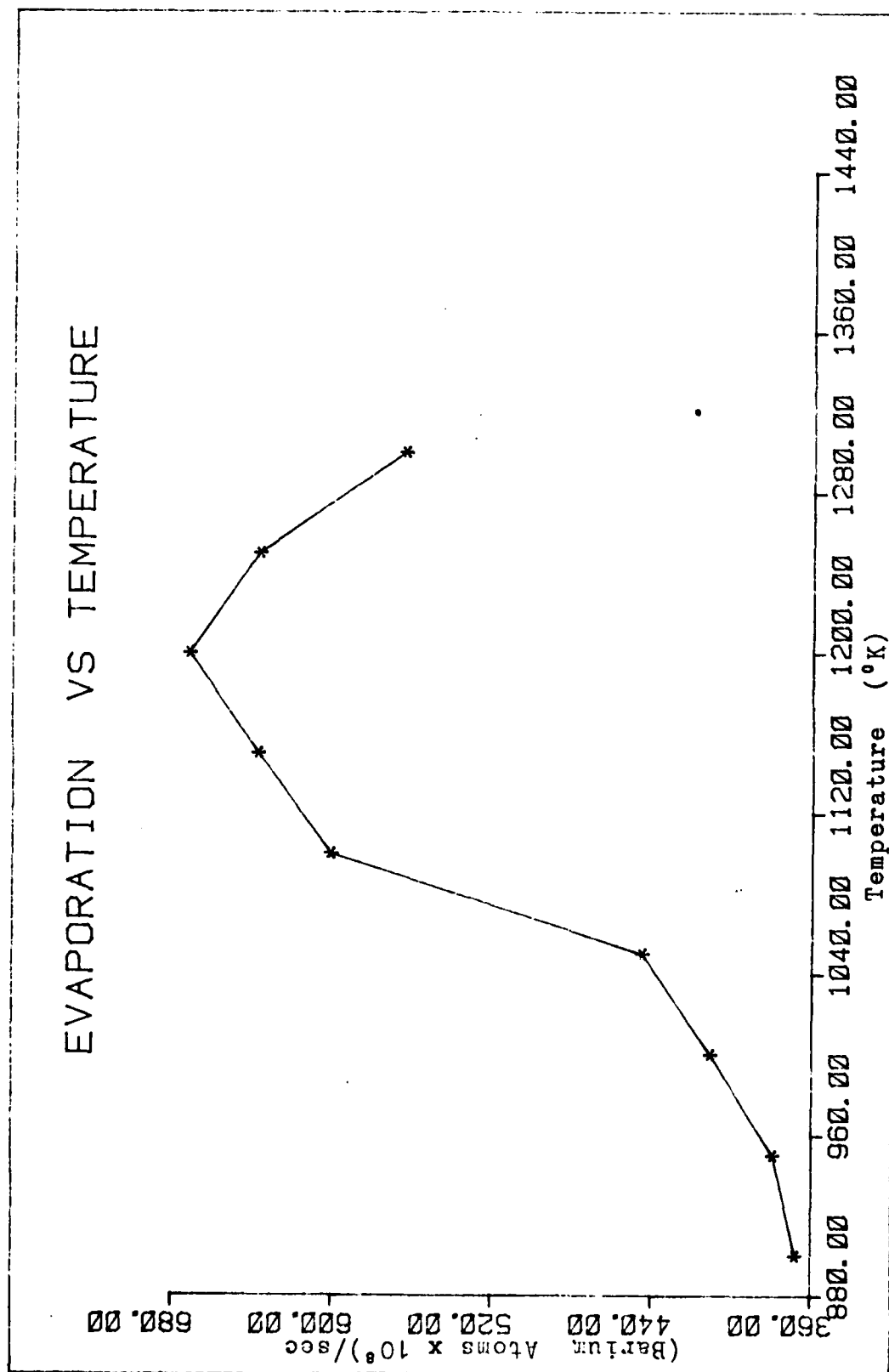


Figure 8. Barium Evaporation Rate versus Cathode Temperature

tained in this experiment agree well with those of Zemyan (Ref 13:51) and served to check the calibration of the system.

Two major features of the relationship are noted. First, below 1100°K, the evaporation rate appears to be increasing in an exponential manner. This is to be expected since the rate of barium evaporation is an exponential function of the cathode temperature given by (Ref 7:28)

$$\ln R_e = C - \frac{5040 \phi}{T} \quad (20)$$

where

R_e is the barium evaporation rate,

C is a constant,

T is the cathode temperature (°K), and

ϕ is the evaporation activation energy; 2.13 eV (Ref 14:163).

The second feature noted is a flattening and actual decrease in the evaporation rate at temperatures above 1100°K. This effect has not been reported before; other research on the evaporation rate using thin film deposition techniques for the measurement of the barium evaporation rate did not indicate a flattening of the evaporation-temperature relationship up to 1600°K (Refs 7:28; 14:159). However, Zemyan's results (Ref 13:51) did show a flattening beginning at 1050°K. There are two possible explanations for the discrepancy in the basic temperature-evaporation characteristic; either some physical process was taking place in the cathode under test in this experiment (which was the same sample used by Zemyan) which actually

reduced the evaporation rate, or else the barium evaporation rate became so large at high temperatures that some of the fluorescent photons were re-absorbed by ground-state barium atoms outside the fluorescing volume, thus reducing the number of photons detected by the PMT. The actual mechanism cannot be deduced from the data. Additional experimentation is necessary to determine the cause of this characteristic.

Evaporation Rate versus Operating Time (Lifetime Test)

The relationship between the barium evaporation rate and the operating time of the cathode with the cathode at a constant 1200°K is shown in figure 9; figure 9a shows the data for the first 10 hours. The characteristics of interest are a rapid decrease in evaporation rate during the first 30 hours, followed by variations about a mean of 7.11×10^9 atoms/sec for the remainder of the test run of 430 hours. The test was terminated at 430 hours due to failure of the cathode's heater.

The Semicon type S cathode used in this experiment is expected to give off excess barium during the first two to five hours of operation (Ref 10) due to excess impregnant on the cathode surface being driven off during the initial heating. This initial "burst" of evaporant is considered a fundamental characteristic of dispenser cathodes and may also be caused by the barium being produced and evaporated more rapidly from pores in the cathode structure which are not contaminated by the products of the activation reaction (Ref 7:28). The data obtained in this experiment reflect this expected behavior.

LIFETIME DATA

* Average 1 - Standard Deviation
uncertainty in N_t (See page 37).

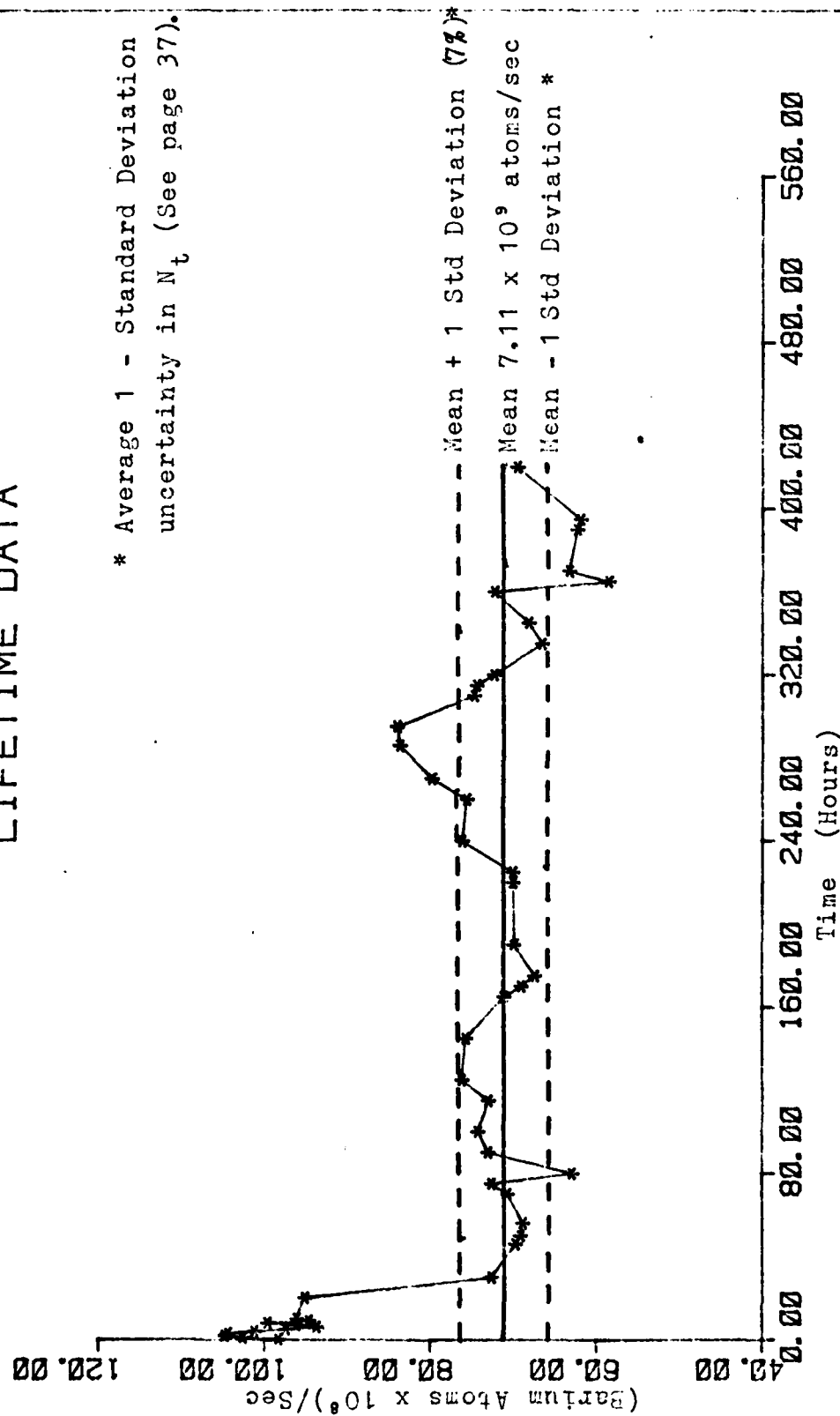


Figure 9. Barium Evaporation Rate versus Cathode Operating Time (Cathode Temperature=1200°K)

10 HOUR LIFETIME DATA

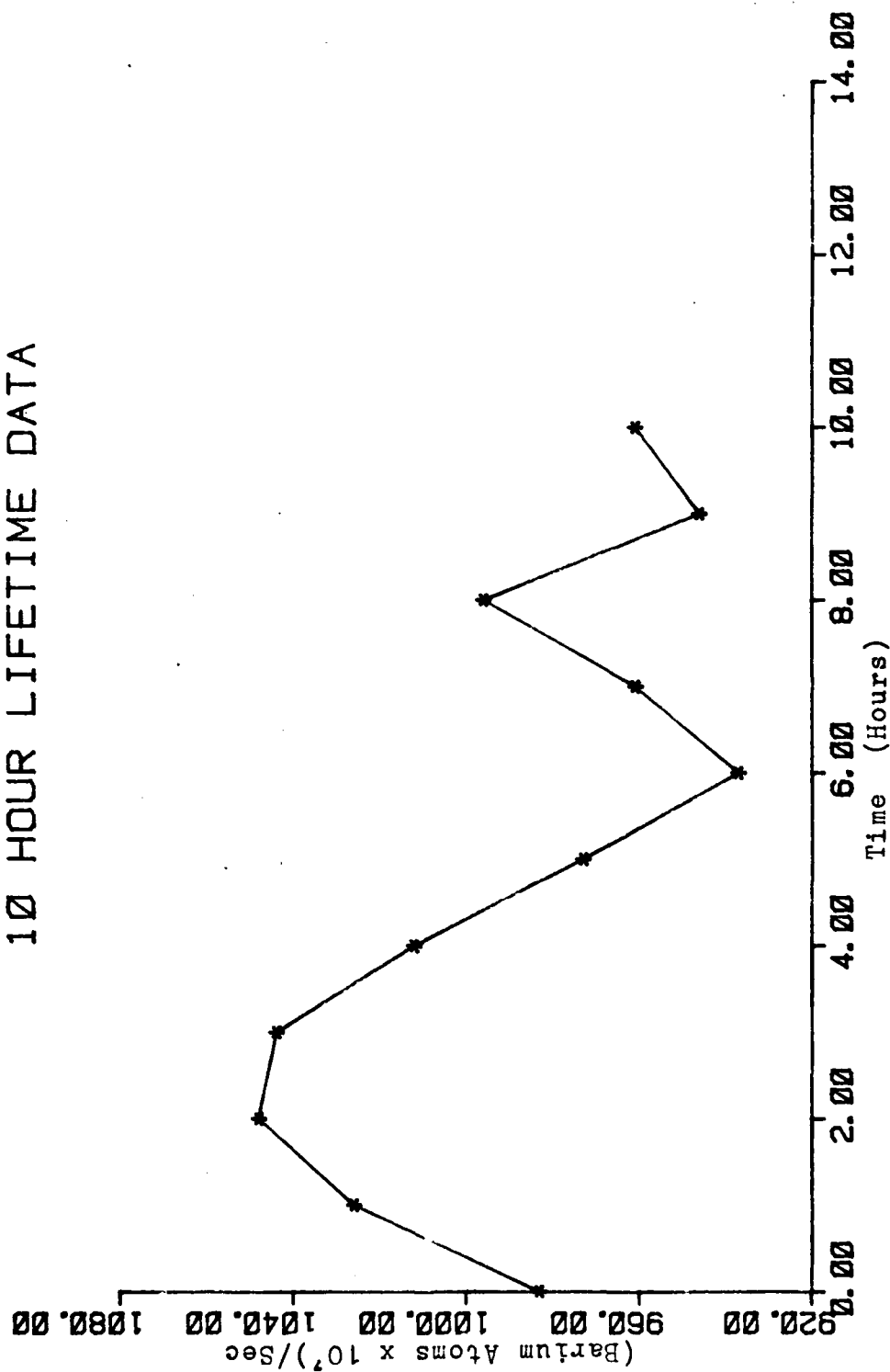


Figure 9a. Barium Evaporation Rate During First Ten Hours of Operation
(Cathode Temperature = 1200°K)

The extended lifetime data is more difficult to interpret in that large fluctuations of the evaporation rate took place and that a general trend is not obvious, although the evaporation rate decreased past 260 hours. The $t^{-\frac{1}{2}}$ behavior of the barium evaporation rate mentioned by Palluel and Shroff (Ref 12:2897), Stupian (Ref 2:31), and Levi (Ref 20:189) is not evident.

A possible explanation of the more constant evaporation rate obtained in this experiment is that, because of the relatively short lifetime over which the evaporation rate was measured and the fairly low cathode temperature (although 1200°K was chosen because the measured evaporation rate was highest at that temperature), the barium reservoir below the cathode surface did not deplete sufficiently to significantly change the evaporation-replenishment balance. Therefore the coverage of the emitting surface by the barium atoms was essentially constant resulting in a constant evaporation rate. This hypothesis could be checked by taking a depth profile of the emitting layer using electron microprobe techniques (Ref 12:2897-2898) to determine the depth to which the barium is depleted. If there is no depleted layer, the evaporation-replenishment balance could be maintained, resulting in a relatively constant evaporation rate. On the other hand, if a strongly depleted region is found it would indicate the decreasing trend of the evaporation rate past 260 hours was an actual decrease and that, if the data had been carried out longer, the $t^{-\frac{1}{2}}$ characteristic would have appeared.

Comments on Accuracy

As was discussed earlier, the standard deviation in the calculated value of the barium evaporation rate ranges from five to eleven percent and averages approximately seven percent. Several assumptions were made to generate the equation relating the fluorescent count rate to the number density of barium.

These were:

1. The atoms evaporating from the cathode had a Maxwellian velocity distribution, with an energy corresponding to the cathode temperature.
2. The method of determining ΩV_{ce} developed by Zemlyan (Ref 13:62-63) and Benham (Ref 20:9) was correct.
3. The barium atoms evaporating from the cathode were emitted vertically and were of a sufficiently low number density so that the ground-state atoms would not re-absorb the photons emitted from the fluorescing volume. Because not all atoms evaporate vertically and since possible re-absorption effects were noted in the temperature runs, these may not be good assumptions; as a result, the calculated evaporation rate is possibly lower than the true evaporation rate, especially at high cathode temperatures.
4. The fluorescing atoms emitted 99 photons since the branching ratio was assumed to be 99% (Ref 13:18). If this was not true, the relationship between the fluorescent count rate and the number density of atoms would have to be changed to account for the different number of photons emitted from each atom (Ref 13:52).

5. The input laser power was sufficient to saturate the barium atoms and cause the 99 photons to be emitted. This experiment used a laser input power of 200 mW which, according to Zemyan's results (Ref 13:45-47), was sufficient to saturate at any cathode temperature.
6. Since the thermocouple on the cathode failed at approximately 50 hours operating time, the cathode temperature was determined using a Leeds and Northrup optical pyrometer. It was assumed that both the thermocouple and the optical pyrometer would give the same reading for the cathode temperature and that the cathode temperature was uniform. By observation, however, and especially as the heater began to fail, localized hot-spots were evident which indicate the emitting surface might not have been at the measured temperature.

VI Conclusions and Recommendations

The following conclusions can be drawn from the results of this experiment;

1. At low temperatures, the measured barium evaporation rate from a Semicon type S cathode increases exponentially with temperature.

2. The evaporation rate versus operating time relationship showed an expected initial high rate of barium evaporation which rapidly fell off to a lower, fairly constant level; the expected $t^{-\frac{1}{2}}$ characteristic was not seen. To determine why the evaporation rate remained constant, the test cathode should be examined by electron microprobe techniques to determine the presence or absence of a barium-depleted region in the barium reservoir.

Additional recommendations, other than that mentioned above are:

1. Decide whether a lifetime test would yield relevant data. If a lifetime test is desired, various steps should be taken to simplify data gathering and ensure the stability of experimental parameters. Such steps include:

- a. Automate the measurement of the fluorescent count rate. Since the photon counter has both analog and RS-232C serial data outputs, the fluorescent count rate can be measured continuously and, if a computer is used to store the data, the necessary calculations can be made automatically.

b. Stabilize the cathode temperature either by use of a thermocouple and amplifier controlling the heater power supply or by use of the background count available from the photon counter; the background count can be converted into an analog signal which can, in turn, control the heater power supply.

c. Stabilize the output power from the dye laser, possibly by use of a photodetector and amplifier controlling the pump laser power.

2. If, on the other hand, a long lifetime test is not considered important, other possible experimental investigations include identification of all species evaporating from the cathode, investigation of the relationship between electron emission and evaporation of any of the identified species, accurate determination of the branching ratio and photon emission rates for the laser-induced fluorescence for any of the species, and the possible effect of re-absorption by the ground-state species on the fluorescent count rate. Each of these possible investigations would provide insights into the cathode operation and the use of laser-induced fluorescence measurements.

Bibliography

1. Strauss, R., J. Bretting, and R. Metivier. "Traveling Wave Tubes for Communication Satellites," Proceedings of the IEEE, 65 (3): 387-400 (March 1977).
2. Stupian, G.W. A Review of the Science and Technology of Cathodes from the Viewpoint of Spacecraft TWT Applications. SD-TR-80-37. Los Angeles AFS, California: Space Division, June 1980 (AD A085778).
3. McKelvey, John. Solid State and Semiconductor Physics. New York: Harper and Row, 1966.
4. Jenkins, R.O. "A Review of Thermionic Cathodes," Vacuum, 19 (8): 353-359 (August 1969).
5. Moses, Alfred. The Practicing Scientist's Handbook. New York: Van Nostrand Reinhold Co., 1978.
6. DeForest, Lee. "A Bit of Electronic History," The Book of Popular Science, 4: 1447-1452. New York: Grolier Society Inc., 1957.
7. Cronin, J.L. "Modern Dispenser Cathodes," IEE Proceedings, 128 (1): 19-32 (February 1981).
8. Green, Michael. Dispenser Cathode Physics. RADC-TR-81-211. Griffiss AFB, New York: Rome Air Development Center, July 1981 (AD A105126).
9. Venema, A. "Dispenser Cathodes: Introduction," Phillips Technical Review, 19 (6): 177-179 (December 1957).
10. Technical Bulletin; Subject: Semicon Dispenser Cathodes. Lexington, Kentucky: Semicon Associates Inc., 1980.
11. Rutledge, W.C., and E.S. Rittner. "Studies on the Mechanism of Operation of the L-Cathode II," Journal of Applied Physics, 28 (2): 167-173 (February 1957).
12. Palluel, P. and A.M. Shroff. "Experimental Study of Impregnated-Cathode Behavior, Emission, and Life," Journal of Applied Physics, 51 (5): 2894-2902 (May 1980).
13. Zemyan, Stephan. Laser Induced Fluorescence of Barium Evaporating from a Dispenser Cathode. MS Thesis AFIT/GNE/PH/82M-13. Wright-Patterson AFB, Ohio: School of Engineering, Air Force Institute of Technology, March 1982.
14. Rittner, E.S., R.H. Ahlert, and W.C. Rutledge. "Studies on the Mechanism of Operation of the L-Cathode I," Journal of Applied Physics, 28: 156-166 (February 1957).

15. Rittner, E.S. "On the Mechanism of Operation of the Type-B Impregnated Cathode," Journal of Applied Physics, 48 (10): 4344-4346 (October 1977).
16. Forman, R. "Comment on the Mechanism of Operation of the Impregnated Tungsten Cathode," Journal of Applied Physics, 50 (3): 1546-1547 (March 1979).
17. Characterization of Tungsten Disoenser Cathodes Using ICS and SIMS. AFML-TR-79-4125. Wright-Patterson AFB, Ohio: Air Force Materials Laboratory, October 1970 (AD A077592).
18. Haas, G.A., H.F. Gray, and R.E. Thomas. "Effects of S, Ba, and C on Impregnated Cathode Surfaces," Journal of Applied Physics, 46 (8): 3293-3301 (August 1975).
19. Rutledge, W.C., A. Milch, and E.S. Rittner. "Measurement of Instantaneous Absolute Barium Evaporation Rates from Dispenser Cathodes," Journal of Applied Physics, 29 (5): 834-839 (May 1958).
20. Levi, R. "Dispenser Cathodes: The Impregnated Cathode," Phillips Technical Review, 19 (6): 136-190 (December 1957).
21. Benham, Vincent. Sodium Concentration Measurements Using Laser Induced Fluorescence. MS Thesis AFIT/GEP/PH/81-1. Wright-Patterson AFB, Ohio: School of Engineering, Air Force Institute of Technology, December 1981 (AD A111138)
22. Fairbank, Jr., W.M., T.W. Hansch, and A.L. Schawlow. "Absolute Measurement of Very Low Sodium Vapor Densities Using Laser Resonance Fluorescence," Journal of the Optical Society of America, 65 (2): 199-204 (February 1975).
23. Jessup, P.E., and F.M. Pipkin. "Measurement of the Lifetime of the $5d6p^1F$ State of Barium," Physical Review A, 20: 269 (July 1979).
24. Lurig, Allen. "Lifetime of the First Excited 1P_1 State of Mg and Ba; HFS of Ba^{137} ," Physical Review, 136: A376-A379 (October 1964).
25. Model 1121A Amplifier-Discriminator Operating and Service Manual. Princeton, New Jersey: E G & G Princeton Applied Research, Inc., 1976.
26. Model 1112 Photon Counter/Processor Operating and Service Manual. Princeton, New Jersey: E G & G Princeton Applied Research, Inc., 1976.
27. George T.V., L. Goldstein, L. Slama, and M. Yokoyama. "Molecular Scattering of Ruby Laser Light," Physical Review, 137: A369-A380 (January 1965).

28. Hengehold, Robert. "Error Analysis," Unpublished Lecture Notes for PH 6.42, Optical Diagnostics Laboratory, School of Engineering, Air Force Institute of Technology, Wright-Patterson AFB, Ohio, 1981.
29. Model 375 Dye Laser with Model 376 or 376E Dye Circulator Instruction Manual. Mountain View, California: Spectra-Physics, Inc., 1980.
30. Kogelnik, H.W., E.P. Ippen, A. Dienes, and C.V. Shank. "Astigmatically Compensated Cavities for CW Dye Lasers," IEEE Journal of Quantum Electronics, QE-8 (3): 373-375 (March 1972).
31. Pedrotti, L.S. and H. Weichel. The Physics of Lasers. Unpublished text. School of Engineering, Air Force Institute of Technology, Wright-Patterson AFB, Ohio, 1980.
32. Yariv, Amnon. Introduction to Optical Electronics, Second Edition. New York, New York: Holt, Rinehart, and Winston, 1976.
33. Precision Optics and Coatings Catalog. Mountain View, California: Spectra-Physics, Inc., 1979.
34. Wolfe, W.L. and G.J. Zissis, Editors. Infrared Handbook. Washington, D.C.: Infrared Information and Analysis Center, Environmental Research Institute of Michigan for the Office of Naval Research, 1978.
35. Yoshida, A., and T. Asakura. "A Simple Technique for Quickly Measuring the Spot Size of Gaussian Laser Beams," Optics and Laser Technology, 8 (6): 273-274 (December 1976).

Appendix A

Calculation of Laser Beam Diameter Over Cathode

A critical element in the calculation of the barium number density and evaporation rate from the measured fluorescent count rate is the knowledge of the laser beam diameter over the cathode. Given the specifications of the dye laser and the knowledge of the elements in the optical path between the laser and the sample, a simple series of calculations gives the beam diameter.

The Spectra-Physics 375 dye laser has a three-mirror, folded cavity configuration (Ref 29:27). An analysis of this type cavity by Kogelnik, et al., (Ref 30:375) gives the beam radius at the output mirror as

$$w_0 \approx (\lambda d_2 / \pi)^{1/2} \quad (\text{A-1})$$

where d_2 is the length of the output arm, in this case 28.7 cm. For a wavelength of 5535\AA , w_0 is 0.22487 mm.

A second parameter required to characterize a TEM_{00} (i.e., Gaussian) laser beam is the complex radius of curvature $\tilde{q}(z)$, where $\tilde{q}(z)$ is defined by

$$\frac{1}{\tilde{q}(z)} = \frac{1}{R(z)} + \frac{i\lambda}{\pi w(z)^2} \quad (\text{A-2})$$

where $R(z)$ is the radius of curvature of the spherical wavefronts at a distance z along the axis of propagation and $w(z)$ is the beam radius at z . Additionally, the basic law of laser propagation is expressed as (Ref 31:4-12)

$$\tilde{q}(z) = \tilde{q}(0) + z \quad (\text{A-3})$$

where $\tilde{q}(0)$ is a known complex radius of curvature at some point $z=z_0$. Since the output mirror of the dye laser is flat, the wavefront at the output mirror is planar; that is $R(\text{output mirror}) = \infty$. Let the position of the output mirror be z_0 ; by equation (A-2),

$$\frac{1}{\tilde{q}(0)} = \frac{1}{\infty} + \frac{i\lambda}{\pi w(0)^2} \quad (\text{A-4})$$

Therefore,

$$\frac{1}{\tilde{q}(0)} = \frac{i\lambda}{\pi w(0)^2} \quad (\text{A-5})$$

and

$$\tilde{q}(0) = -i \frac{\pi w(0)^2}{\lambda} \quad (\text{A-6})$$

Combining equations (A-1) and (A-6),

$$\tilde{q}(0) = -id_2 \quad (\text{A-7})$$

for the three-mirror cavity. Therefore, $\tilde{q}(0) = -28.7i$ cm at the output mirror. Given the beam radius and complex radius of curvature at the output mirror, the same quantities can be determined for any position along the optical path.

To determine these parameters, the ABCD law (Ref 32:36-37) is used which states

$$\tilde{q}_2 = \frac{A\tilde{q}_1 + B}{C\tilde{q}_1 + D} \quad (\text{A-8})$$

where A, B, C, and D are the elements of a 2 x 2 matrix characterizing the optical path between the positions z_1 and z_2 such that $\tilde{q}_1 = \tilde{q}(z_1)$ and $\tilde{q}_2 = \tilde{q}(z_2)$. In turn, the matrix $\begin{pmatrix} A & B \\ C & D \end{pmatrix}$ is the product of the individual $\begin{pmatrix} A & B \\ C & D \end{pmatrix}$ matrices for each element in the optical path. That is, for a k-element optical system

$$\begin{pmatrix} A & B \\ C & D \end{pmatrix}_{\text{system}} = \prod_{i=1}^k \begin{pmatrix} A_i & B_i \\ C_i & D_i \end{pmatrix} \quad (\text{A-9})$$

For the system used in this experiment (figure 10), the expansion of equation (A-9) is

$$\begin{pmatrix} A & B \\ C & D \end{pmatrix}_{\text{system}} = \begin{pmatrix} A & B \\ C & D \end{pmatrix}^{T_5} \begin{pmatrix} A & B \\ C & D \end{pmatrix}^{L_1} \begin{pmatrix} A & B \\ C & D \end{pmatrix}^{T_4} \begin{pmatrix} A & B \\ C & D \end{pmatrix}^{M_2} \begin{pmatrix} A & B \\ C & D \end{pmatrix}^{T_3} \begin{pmatrix} A & B \\ C & D \end{pmatrix}^{M_1} \begin{pmatrix} A & B \\ C & D \end{pmatrix}^{T_2} \begin{pmatrix} A & B \\ C & D \end{pmatrix}^{T_1} \quad (\text{A-10})$$

The matrix for a translation is

$$\begin{pmatrix} A & B \\ C & D \end{pmatrix}^{T_i} = \begin{pmatrix} 1 & D/n \\ 0 & 1 \end{pmatrix} \quad (\text{A-11})$$

where D is the translation distance and n is the refractive index of the medium through which the translation occurs. For a lens of focal length f, the matrix is

$$\begin{pmatrix} A & B \\ C & D \end{pmatrix}^{L_i} = \begin{pmatrix} 1 & 0 \\ -1/f & 1 \end{pmatrix} \quad (\text{A-12})$$

and for a reflection from mirror M_i with a radius of curvature R_i

$$\begin{pmatrix} A & B \\ C & D \end{pmatrix}^{M_i} = \begin{pmatrix} 1 & 0 \\ -2/R_i & 1 \end{pmatrix} \quad (\text{Ref 32:20}) \quad (\text{A-13})$$

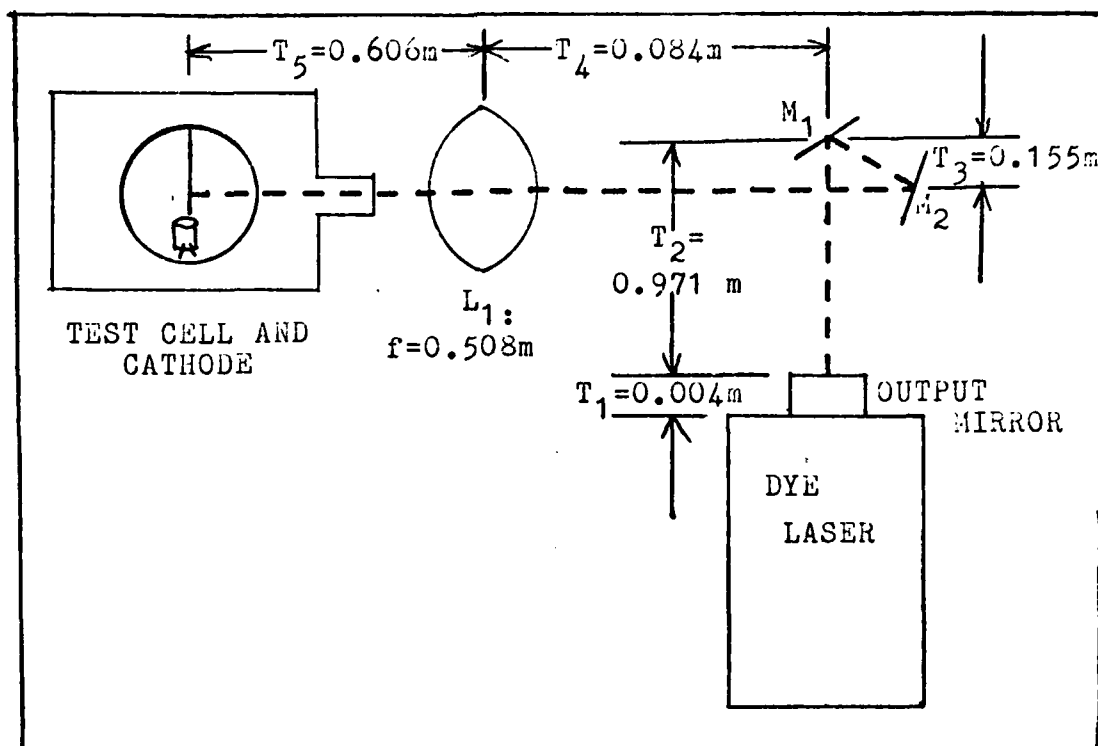


Figure 10. Laser Beam Path Schematic (Lengths not to scale)

Therefore, substituting the translation lengths T_1 through T_5 and the focal length of the lens L_1 into equation (A-10), the system matrix is

$$\begin{bmatrix} A & B \\ C & D \end{bmatrix}_{\text{system}} = \begin{bmatrix} 1 & 0.606\text{m} \\ 0 & 1 \end{bmatrix} \begin{bmatrix} 1 & 0 \\ -1/0.508\text{m} & 1 \end{bmatrix} \begin{bmatrix} 1 & 0.084\text{m} \\ 0 & 1 \end{bmatrix} \begin{bmatrix} 1 & 0 \\ -2/R_2 & 1 \end{bmatrix} \\ \begin{bmatrix} 1 & 0.155\text{m} \\ 0 & 1 \end{bmatrix} \begin{bmatrix} 1 & 0 \\ -2/R_1 & 1 \end{bmatrix} \begin{bmatrix} 1 & 0.971\text{m} \\ 0 & 1 \end{bmatrix} \begin{bmatrix} 1 & 4 \times 10^{-3}\text{m/n} \\ 0 & 1 \end{bmatrix} \quad (\text{A-14})$$

Since M_1 and M_2 are flat mirrors, R_1 and $R_2 = \infty$. Therefore, $-2/R_1 = 0$; as a result, the matrices for the mirrors reduce to identity matrices and can be ignored for the multiplication.

The substrate of the output mirror is optical grade fused silica (Ref33:9) with a refractive index of 1.46 (Ref 34:7-59,7-60).

Thus, the matrix for translation through the output mirror substrate is $\begin{pmatrix} 1 & 0.004\text{m}/1.46 \\ 0 & 1 \end{pmatrix} = \begin{pmatrix} 1 & 0.0027\text{m} \\ 0 & 1 \end{pmatrix}$, and the matrix for the entire system, by carrying out the multiplication in (A-14) is

$$\begin{pmatrix} A & B \\ C & D \end{pmatrix}_{\text{system}} = \begin{pmatrix} -0.1929 & 0.37206\text{m} \\ -1/0.508\text{m} & -1.3872 \end{pmatrix} \quad (\text{A-15})$$

Then, applying (A-15) to (A-9) yields

$$\tilde{q}_{\text{cathode}} = \frac{37.206 + 5.536i}{-1.387 + 0.565i} \text{ cm} \quad (\text{A-16})$$

so that

$$\frac{1}{\tilde{q}_{\text{cathode}}} = (-0.034 + 0.020i)/\text{cm} \quad (\text{A-17})$$

Equating imaginary parts of (A-2) and (A-17) gives

$$w_{\text{cathode}}^2 = \frac{5535 \times 10^{-8} \text{ cm}}{(\pi)(0.020)/\text{cm}} = 8.69 \times 10^{-4} \text{ cm}^2 \quad (\text{A-18})$$

or $w_{\text{cathode}} = 0.029 \times 10^{-2} \text{ m} = 0.29 \text{ mm}$ beam radius over the cathode. Therefore, the beam diameter over the cathode is 0.58mm. The result was checked by measuring the beam diameter 30 cm from the output mirror using the thin-wire method of Yoshida and Asakura (Ref 35:273-274). The ABCD matrix for the path was calculated, and the beam diameter was found to be the expected value.

Appendix B

TABULATED DATA

The tables included in this appendix give the numerical values of the fluorescent photon count rate R_f , the barium number density N_t , and the evaporation rate R_e , along with the standard deviations of R_f (σ_{R_f}) and R_e (σ_{R_e}) for both the temperature and operating time tests.

Table 1

TEMPERATURE TEST

T_{cathode} (°K)	R_f ($10^4/\text{sec}$)	σ_{R_f} ($10^4/\text{sec}$)	N_t ($10^{12}/\text{m}^3$)	R_e ($10^{10}/\text{sec}$)	σ_{R_e} ($10^{10}/\text{sec}$)
900	1.006	0.0342	3.455	3.677	0.152
950	1.038	0.0203	3.468	3.792	0.115
1000	1.124	0.0176	3.661	4.107	0.114
1050	1.217	0.0626	3.870	4.449	0.250
1100	1.644	0.0456	5.107	6.008	0.212
1150	1.741	0.0318	5.298	6.375	0.180
1200	1.837	0.0327	5.464	6.715	0.190
1250	1.741	0.0782	5.073	6.634	0.318
1300	1.543	0.0645	4.408	5.638	0.266

Table 2

OPERATING TIME TEST

Time (hours)	R_f ($10^4/\text{sec}$)	σ_{R_f} ($10^4/\text{sec}$)	N_t ($10^{11}/\text{m}^3$)	R_e ($10^{10}/\text{sec}$)	σ_{R_e} ($10^{10}/\text{sec}$)
0	2.690	0.0602	8.000	0.983	0.037
1	2.806	0.0873	8.346	1.026	0.044
2	2.866	0.0526	8.524	1.048	0.036
3	2.856	0.1101	8.494	1.044	0.051
4	2.769	0.0516	8.235	1.012	0.035
5	2.663	0.0494	7.920	0.973	0.072
6	2.563	0.0541	7.623	0.937	0.069
7	2.630	0.2100	7.822	0.961	0.082
8	2.726	0.0851	8.108	0.996	0.049

Table 2
OPERATING TIME TEST
(Continued)

Time (Hours)	R_f ($10^4/\text{sec}$)	σ_{R_f} ($10^4/\text{sec}$)	N_t ($10^{11}/\text{m}$)	R_e ($10^{10}/\text{sec}$)	σ_{R_e} ($10^{10}/\text{sec}$)
9	2.694	0.0851	8.012	0.985	0.043
10	2.630	0.0630	7.822	0.961	0.036
20	2.601	0.0867	7.736	0.951	0.042
30	1.986	0.3039	5.907	0.726	0.116
46	1.908	0.0565	5.675	0.697	0.029
50	1.891	0.1110	5.624	0.691	0.046
56	1.882	0.0297	5.598	0.688	0.023
70	1.935	0.0415	5.755	0.707	0.016
75	1.986	0.0471	5.907	0.726	0.017
80	1.720	0.0749	5.118	0.629	0.024
90	1.996	0.0623	5.937	0.730	0.032
100	2.029	0.0711	6.035	0.742	0.021
115	1.997	0.0920	5.940	0.730	0.040
125	2.084	0.0446	6.198	0.762	0.028
145	2.070	0.0704	6.157	0.757	0.034
165	1.945	0.0662	5.785	0.711	0.032
170	1.887	0.0649	5.612	0.690	0.031
175	1.843	0.0347	5.482	0.674	0.024
190	1.911	0.0708	5.684	0.699	0.033
220	1.916	0.0666	5.697	0.700	0.032
225	1.915	0.1302	5.694	0.700	0.053
240	2.083	0.1943	6.193	0.761	0.075
260	2.066	0.1193	6.143	0.755	0.050
270	2.180	0.0476	6.482	0.797	0.029
286	2.291	0.0825	6.812	0.837	0.039
295	2.298	0.0589	6.833	0.840	0.033
310	2.044	0.0698	6.077	0.747	0.034
315	2.035	0.0569	6.051	0.744	0.031
320	1.980	0.0537	5.887	0.723	0.029
335	1.819	0.0454	5.408	0.665	0.026
345	2.864	0.0473	5.542	0.681	0.027
360	1.974	0.0378	5.872	0.722	0.026
365	1.600	0.0573	4.757	0.585	0.028
370	1.731	0.0244	5.149	0.633	0.021
390	1.705	0.0737	5.069	0.623	0.033
395	1.694	0.1586	5.036	0.619	0.062
420	1.901	0.1237	5.652	0.695	0.051

Vita

Eugene Francis Kasper was born on 18 September 1952 in Newark, New Jersey. His family moved to southern California where he graduated from the Don Bosco Technical Institute, majoring in electronics, in 1970. He graduated from the University of Notre Dame in 1974 with the degree of Bachelor of Science, Electrical Engineering. After working at Lear-Siegler in Anaheim, California on the ADM-2 and ADM-3 data terminal projects, he entered active duty in the Air Force in December 1974. He spent six years as an Air Force helicopter pilot and flight instructor in Korea, Arizona, and New Mexico. He was selected to attend the Air Force Institute of Technology in 1980. He is a member of the IEEE and its Computer, Control Systems, Aerospace Electronics Systems, and Quantum Electronics and Applications societies. He is married to the former Chong Kyong Ae of Sakok-Myon, Republic of Korea, and has two daughters. His permanent address is 14382 Red Hill Avenue #55, Tustin, California 92680.

UNCLASSIFIED

SECURITY CLASSIFICATION OF THIS PAGE (When Data Entered)

REPORT DOCUMENTATION PAGE		READ INSTRUCTIONS BEFORE COMPLETING FORM								
1. REPORT NUMBER AFIT/GEO/PH/82D-5	2. GOVT ACCESSION NO.	3. RECIPIENT'S CATALOG NUMBER								
4. TITLE (and Subtitle) MEASUREMENT OF BARIUM EVAPORATION FROM A DISPENSER CATHODE USING LASER-INDUCED FLUORESCENCE		5. TYPE OF REPORT & PERIOD COVERED MS Thesis								
		6. PERFORMING ORG. REPORT NUMBER								
7. AUTHOR(s) EUGENE F. KASPER Captain USAF		8. CONTRACT OR GRANT NUMBER(s)								
9. PERFORMING ORGANIZATION NAME AND ADDRESS AIR FORCE INSTITUTE OF TECHNOLOGY (AFIT-EN) WRIGHT-PATTERSON AFB OHIO 45433		10. PROGRAM ELEMENT, PROJECT, TASK AREA & WORK UNIT NUMBERS								
11. CONTROLLING OFFICE NAME AND ADDRESS		12. REPORT DATE DECEMBER 1982								
		13. NUMBER OF PAGES 66								
14. MONITORING AGENCY NAME & ADDRESS (if different from Controlling Office)		15. SECURITY CLASS. (of this report) UNCLASSIFIED								
		15a. DECLASSIFICATION/DOWNGRADING SCHEDULE								
16. DISTRIBUTION STATEMENT (of this Report) APPROVED FOR PUBLIC RELEASE; DISTRIBUTION UNLIMITED										
17. DISTRIBUTION STATEMENT (of the abstract entered in Block 20, if different from Report)										
18. SUPPLEMENTARY NOTES <p>Approved for public release; LAW AFR 190-17. LYNN E. WOLAVER Dean for Research and Professional Development Air Force Institute of Technology (AIG) Wright-Patterson AFB OH 45433</p> 6 JAN 1983										
19. KEY WORDS (Continue on reverse side if necessary and identify by block number) <table border="0"> <tr> <td>BARIUM</td> <td>ELECTRON TUBES</td> </tr> <tr> <td>CATHODES</td> <td>TRAVELLING WAVE TUBES</td> </tr> <tr> <td>THERMIONIC CATHODES</td> <td>LASER</td> </tr> <tr> <td>DISPENSER CATHODES</td> <td>LASER-INDUCED FLUORESCENCE</td> </tr> </table>			BARIUM	ELECTRON TUBES	CATHODES	TRAVELLING WAVE TUBES	THERMIONIC CATHODES	LASER	DISPENSER CATHODES	LASER-INDUCED FLUORESCENCE
BARIUM	ELECTRON TUBES									
CATHODES	TRAVELLING WAVE TUBES									
THERMIONIC CATHODES	LASER									
DISPENSER CATHODES	LASER-INDUCED FLUORESCENCE									
20. ABSTRACT (Continue on reverse side if necessary and identify by block number) <p>The rate of evaporation of barium atoms from a thermionic dispenser cathode is measured as a function of cathode temperature and operating time using laser-induced fluorescence techniques. A continuous-wave dye laser is tuned to the 553.5 nm barium I transition. The laser beam is passed over a heated cathode and the resulting fluorescence is detected and measured using photon counting techniques. The evaporation rate is calculated from the measured fluorescent intensity. (over)</p>										

UNCLASSIFIED

SECURITY CLASSIFICATION OF THIS PAGE (When Data Entered)

UNCLASSIFIED

SECURITY CLASSIFICATION OF THIS PAGE (When Data Entered)

The results indicate that, for a Semicon type S cathode, the evaporation rate increases until the cathode temperature reaches 1200°K ; above this temperature, the measured rate decreases. The lifetime data indicates that, after an initially high rate for the first 30 hours, the evaporation rate becomes approximately constant at 7.11×10^7 atoms/sec for the 420 hour duration of the test. The cathode heater failed at 430 hours.